

The beads-on-string structure of viscoelastic threads

By **Christian Clasen**^{1,5}, **Jens Eggers**^{2,6}, **Marco A. Fontelos**³, **Jie Li**⁴,
and **Gareth H. McKinley**¹

¹Hatsopoulos Microfluids Lab, Department of Mechanical Engineering, MIT, Cambridge, Mass. 02139, USA

²Universität Gesamthochschule Essen, Fachbereich Physik, 45117 Essen, Germany

³Departamento de Ciencia e Ingeniería, Universidad Rey Juan Carlos, C/ Tulipán S/N, 28933 Móstoles, Madrid, Spain.

⁴BP Institute & Engineering Department, University of Cambridge, Madingley Road Cambridge, CB3 0EZ, United Kingdom

⁵present address: Institut für Technische und Makromolekulare Chemie, Bundesstr. 45, 20146 Hamburg, Germany

⁶present address: School of Mathematics, University of Bristol, University Walk, Bristol BS8 1TW, United Kingdom

(Received ?? and in revised form ??)

By adding minute concentrations of a high molecular weight polymer, liquid jets or bridges collapsing under the action of surface tension develop a characteristic shape of uniform threads connecting spherical fluid drops. In this paper, high-precision measurements of this beads-on-string structure are combined with a theoretical analysis of the limiting case of large polymer relaxation times, for which the evolution can be divided into two distinct regimes. This excludes the very late stages of the evolution, for which the polymers have become fully stretched. For times smaller than the polymer relaxation time, over which the beads-on-string structure develops, we give a simplified local description, which still contains the full complexity of the problem. At times much larger than the relaxation time, we show that the solution consists of exponentially thinning threads connecting almost spherical drops. Both experiment and theoretical analysis of a one-dimensional model equation reveal a self-similar structure of the corner where a thread is attached to the neighbouring drops.

1. Introduction

Understanding the behaviour of polymeric free-surface flows is of enormous importance for a wide variety of applications in the chemical processing, food and consumer products industries. Operations such as ink jet printing, spraying of fertilizers, paint-leveling, misting, bottle-filling and roll coating are all controlled by interactions between the non-Newtonian stresses in the bulk and capillary stresses at the deformable free-surface. Long-chained macromolecules are also ubiquitous in biological fluids, and very significantly affect the corresponding free-surface dynamics. If one places a small drop of saliva between two fingers and pulls them apart, the resulting liquid bridge does not collapse, but an extremely fine thread remains for several seconds. The lifetime of this bridge is intimately connected with the molecular weight and conformation of the proteins (mucins) and hormones in the saliva. Measurement of such filament lifetimes in

biofluids such as mucus or saliva can be used as a fertility indicator Kopito & Kosasky (1979).

A number of recent studies have promulgated the idea of using the capillarity-induced thinning of a liquid filament as a rheometric device for quantifying the properties of complex fluids in predominantly extensional flows (Bazilevsky et al. (1990), Stelter et al. (2000), Tripathi et al. (2000)). A typical configuration is shown in Figure 1. A liquid bridge of the fluid to be tested is initially formed between two coaxial cylindrical plates and a step uniaxial strain is then imposed on the bridge to extend it beyond the static (Plateau) stability limit. The liquid filament then undergoes a capillary-thinning process towards a final breakup event. The no-slip boundary condition at the endplates retards the radial flow near the end plates and thus imposes a well-defined initial axial perturbation or 'neck' on the liquid column which controls the location of the subsequent necking process. The time evolution in the local filament radius is monitored optically using either a laser micrometer or high-speed video imaging. To convert such measurements of filament evolution into an extensional viscosity or other material function characterizing free-surface extensional flows of complex fluids, it is necessary to understand the balance of forces acting on the fluid filament. Capillary pressure drives the thinning process whilst viscous and elastic stresses (plus gravity) resist the necking of the fluid thread. The slenderness of the fluid thread induced by the step strain means that a one-dimensional approximation to the equations can be useful and the large viscosity of many polymeric fluid systems means that inertial effects can often be neglected over the majority of the capillary-thinning process. Entov & Hinch (1997) provide a detailed discussion of the evolution of a cylindrical thread of viscoelastic fluid undergoing capillary-driven breakup. A central result of both this work and earlier studies is that there can be a lengthy intermediate regime in which inertial, viscous and gravity forces are all negligible and elastic and capillary forces balance each. In this regime the local extension rate in the neck is constant and the radius of the filament decreases exponentially in time. Measurement of this rate of thinning enables a direct determination of the characteristic relaxation time of the viscoelastic fluid. Such observations have been found to be in quantitative agreement with data obtained in extensional rheometers (Anna & McKinley (2001)).

This local elasto-capillary balance has also been observed in other experimental configurations including breakup of forced polymeric jets (Christanti & Walker (2002)) and gravity-driven drop formation in viscoelastic polymer solutions (Amarouchene et al. (2001), Cooper-White et al. (2002)). In these experiments, the fluids typically have low viscosities and the initial stages of the process exhibit characteristics of a self-similar solution resulting from a balance between capillary pressure and fluid inertia (Day et al. (1998)) including a power-law decrease in the minimum radius. The rapid growth in viscoelastic stresses within the fluid neck leads to a cross-over to an exponential decrease in the minimum filament radius with time which is a hallmark of the elasto-capillary balance. However additional details of the self-similar solution (such as the spatial profile of the filament) are presently unknown. By contrast, in the absence of polymeric additives, the cross-over to a self-similar 'universal solution' balancing viscosity, inertia and capillarity are now well-explored (Eggers (1997), Rothert et al. (2001), Chen et al. (2002)).

On close examination of a thinning viscoelastic jet, a string of tiny droplets can often be distinguished. This 'beads on a string' phenomenon was first described in Goldin et al. (1969), and has been reproduced in numerical simulations by Bousfield et al. (1986). A representative image of this viscoelastic jet break-up process is shown in 2. The jet consists of a series of cylindrical ligaments connecting spherical beads. As the jet is

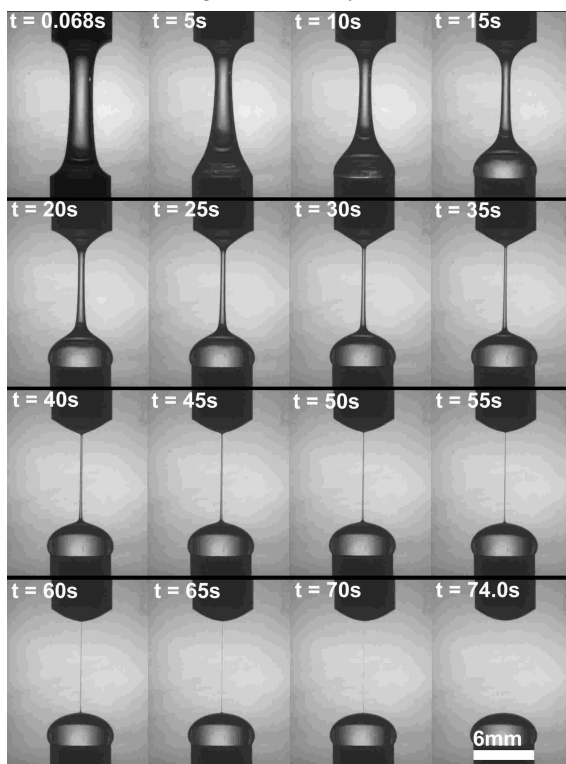


FIGURE 1. Experimental images of a collapsing liquid bridge of polymer solution in a viscous solvent (plate radius $R_0 = 3\text{mm}$, distance 13.8mm). The surface tension is $\gamma = 37\text{mN/m}$, the density $\rho = 1026\text{kg/m}^3$. The solvent and polymeric contributions to the viscosity are $\eta_s = 65.2\text{Pas}$ and $\eta_p = 9.8\text{Pas}$, respectively, the polymer timescale is $\lambda = 8.1\text{s}$. Relative to the capillary timescale $\tau = \sqrt{\rho R_0^3/\gamma}$ this results in a Deborah number of $De = 296$.

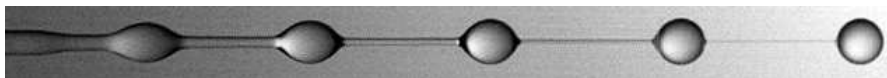


FIGURE 2. High speed videoimage of a jet of dilute (0.01 wt%) aqueous polyacrylamide solution (surface tension $\gamma = 62\text{mN/m}$) undergoing capillary thinning. The sharp-edged jet orifice is at the left of the image (radius $R_0 = 0.30\text{mm}$) and the free jet velocity is 30cm/s . The polymeric contribution to the viscosity is $\eta_p = 0.0119\text{Pas}$, and the polymer timescale is found to be $\lambda = 0.012\text{s}$. This corresponds to a Deborah number of $De = 18.2$.

convected from left to right, fluid is forced by capillarity from the thinning ligaments into the spherical droplets

Most analytical studies of this structure have been performed using simplifying assumptions about the slenderness of the liquid jet, see Yarin (1993) for a review. However, despite a considerable number of studies (see e.g. Goren & Gottlieb (1982), Entov & Yarin (1984), Bousfield et al. (1986), Forest et al. (1990), Shipman et al. (1991), Larson (1992), Renardy (1994), Renardy (1995), Chang et al. (1999)) a full analytical description of the beads-on-string phenomenon is still open, even in the context of one-dimensional models.

In this paper we seek a self-similar solution that encompasses the elasto-capillary balance documented in experimental observations in liquid bridges, pinching drops and thin-

ning jets. We follow the spirit of some of the earlier work by employing two simplifying assumptions:

First, we will consider the simplest canonical model for a dilute polymer solution, the so-called Oldroyd-B model (e.g. Bird et al. (1987)). This model is most easily derived from kinetic theory by treating a dilute solution of polymer chains as a suspension of non-interacting dumbbells, i.e. as two point masses or ‘beads’ at which the viscous drag from the solvent is imparted, connected by a Hookean spring. The beads are assumed to be convected by the flow without slip, so in the extensional flow of a pinching thread, the beads are pulled apart, stretching the spring. In return, the dumbbell imparts a stress on the fluid, which results in a polymeric contribution to the stress tensor which is proportional to the force in the spring. The simplifying assumptions of a Hookean dumbbell are that the polymer chain exhibits a single relaxation time λ , and that the spring is infinitely stretchable. The one-dimensional analysis of Entov & Hinch (1997) considered the more general case of a spectrum of relaxation times (corresponding to a non-interacting suspension of dumbbells with different spring constants). Their analysis showed that the rate of stretching in the liquid thread is governed by the dumbbells with the longest time constant and that all other modes relax and do not contribute to the dominant balance, so this approximation of a single relaxation time is not considered to be too limiting. Furthermore, a number of recent experimental studies (e.g. Spiegelberg et al. (1996), Amarouchene et al. (2001), Anna & McKinley (2001)) have utilized model dilute polymer solutions which are indeed very well described by a single time scale over a wide range of extensions. The additional assumption of infinite extensibility is bound to break down even for very long polymers as the trajectories of the two beads diverge exponentially in an extensional flow. In fact, it has been shown by Renardy (1994) for the model to be treated in this paper (and neglecting inertia) that a thread can *never* break up in finite time. In our study, we therefore disregard the final stages of breakup where the finite length of the polymers begins to affect the necking process. This regime has been considered by Entov & Hinch (1997), and the filament radius ultimately decreases linearly in time.

The second simplifying assumption is that we are treating the flow inside the fluid thread as effectively one-dimensional (e.g. Forest et al. (1990)). This is consistent as long as the shape of the liquid column remains slender, i.e. the characteristic radial variations are small compared to the variation in the axial direction. This assumption is problematic near the ends of the fluid drops in the beads-on-string structure. Following Eggers & Dupont (1994), we hope to at least partially deal with this problem by keeping the *full* expression for the mean curvature in the Laplace pressure, which drives the breakup. This makes spherical drops exact static solutions of the equations, and ensures that at least the surface tension terms are correctly accounted for.

We are left with a model that treats the liquid column as a set of one-dimensional continuum equations for the fluid flow coupled with equations describing the state of stress of the polymer chains in solution. A typical experimental situation would be that of a jet ejected from a nozzle, or a liquid bridge held between two circular end-plates. In all of the following, we will choose the initial bridge or jet radius R_0 as a unit of length, and the corresponding capillary time $\tau = (\rho R_0^3 / \gamma)^{1/2}$ as unit of time, where γ is the surface tension and ρ the density of the fluid. If $R_0 \approx 1\text{mm}$, τ is about 4 ms for a water-based solvent. Note that for a high viscosity fluid (also treated in this paper) other time scales such as the viscous scale $\tau_\eta = \eta R_0 / \gamma$ arising from a balance of surface tension and viscosity, might be more appropriate. However, to avoid confusion we will consistently use the inertial-capillary time scale. There still remain three independent dimensionless

parameters in the problem. The time scale λ of the polymer is conventionally called a Deborah number, De , when made dimensionless with the characteristic time scale of the system. In the present study we thus have $De = \lambda/\tau$. Note that the Deborah number is ‘intrinsic’ to the fluid thread because it is defined entirely in terms of material and geometric parameters. It does not contain the rate of stretching in the fluid, since the flow is not forced but is free to select its own rate of stretching, which may be spatially and/or temporally inhomogeneous. The other two dimensionless parameters represent the relative contributions of viscous stresses from the solvent and the polymer. There are a number of possible representations for these parameters. The total dynamical viscosity for a dilute polymer solution characterized by the Oldroyd-B model is given by $\eta_0 = \eta_s + \eta_p$ and the relative importance of viscous effects can thus be characterized by the Ohnesorge number $Oh = \eta_0/\sqrt{\rho\gamma R_0}$ and the solvent viscosity ratio $S = \eta_s/\eta_0$. An alternative representation which we use below is to separate the relative dimensionless contributions of the kinematic viscosity $\nu_s = OhS$ of the solvent, and the polymeric contribution to the viscosity $\nu_p = Oh(1 - S)$. All these material constants have been made dimensionless using R_0 , γ and τ as the characteristic scales.

Even if one only considers the case of a fixed initial condition, and neglects gravity (say in a liquid bridge configuration), the problem is still one of daunting complexity. In particular, the behaviour of the liquid bridge need not be spatially uniform throughout: in some regions the rate v' at which fluid elements are stretched may be smaller than $1/(2De)$. In this case polymer relaxation overcomes flow stretching, and the polymers remain coiled, leading to Newtonian-like behaviour. In other parts of the flow stretching overpowers relaxation, and the polymers become stretched in unison with the exponentially diverging paths of fluid elements. In these regions, the polymeric contribution to the stress grows accordingly, and threads form. The transition from a flow regime with $2v'De < 1$ to one with $2v'De > 1$, where exponential stretching of polymers may occur, has been called the ‘coil-stretch’ transition by deGennes (1974).

It is very difficult to describe this complexity in full generality, so in the following we will restrict ourselves to the case of large $De \gg 1$, implying that the non-Newtonian polymer contribution is significant at all times. Physically this means that De is much larger than the initial time scale of the liquid bridge’s evolution, which is set by the linear stability of the fluid thread. At low viscosities, $Oh = \nu_s + \nu_p < 1$, this time scale is $O(1)$ by virtue of the chosen time scale for non-dimensionalization. By contrast, for fluids with large viscosities it is set by $\tau_\eta = \tau/Oh$, and we thus require $De/Oh \gg 1$. Note that with the present scaling, $1/Oh^2$ is the ratio of the external length scale R_0 and the intrinsic scale of the fluid, $\ell_\nu = \nu^2/(\gamma\rho)$.

With these assumptions, we can divide the transient evolution of the jet into distinct stages as shown schematically in Figure 3. The dimensional time \tilde{t} elapsed is scaled with both the polymer relaxation time λ and the appropriate time scale for evolution of the fluid thread τ_{ch} (which depends on the value of the Ohnesorge number). Fluid elements in the jet evolve along pathlines of constant slope $\lambda/\tau_{ch} = De_{ch}$. In each regime, we can provide a simplified description by balancing the dominant terms in the governing equations. The focus of this paper will be on the sector characterized by large De_{ch} .

In the early elastic time regime, $t \ll 1 \ll De$, there is no significant decay of polymer stretching. The fluid thus responds as a neo-Hookean elastic material. This allows the effect of the polymers to be written as a *local* contribution to the pressure, given in terms of the interface shape (i.e. the local accumulated strain) alone. The parameter determining the magnitude of this contribution is the dimensionless elastic modulus of the material $G = \nu_p/De$, which is (up to universal constants) proportional to the polymer *concentration*. Depending on the viscosity, the dynamics of the bridge can be

quite complex. In particular, for low viscosities, capillary waves can travel along threads and rebound off drops (Li & Fontelos (2003)). Threads are also shown to support elastic waves.

For $De \gg t \gg 1$, as polymers become sufficiently stretched to counter surface tension forces, the simplified, local system of equations converges to a *stationary* solution, maintained by the stress in the polymers with no possibility of relaxation. This stationary solution, originally found by Entov & Yarin (1984), already exhibits the beads-on-string structure, but with a thread of radius $h_{thread} = (G/2)^{1/3}$ to be computed in section 3.2. The transition of the initial evolution to the region marked “quasi-static” in Fig. 3 thus occurs approximately when this radius is reached. The name “quasi-static” refers to the fact that the solution can only be regarded as stationary on time scales much smaller than the polymer relaxation time.

Indeed, to proceed beyond this stage one has to take the viscoelastic relaxation of the polymer chains into account. The structure of the solution is that of cylindrical filaments which thin at an exponential rate $\exp(-t/3De)$ as a result of the local balance between elasticity and capillarity. The filaments connect an arbitrary distribution of droplets, which approach a static, spherical shape. A similarity solution describes the crossover between the cylindrical thread and the neighbouring droplet. Towards the thread, the solution asymptotes towards a constant thickness, in the direction of the drop it fits onto the spherical shape of the drop. Since the asymptotic shape is that of threads of vanishing radius connecting perfect circles, a corner develops, with the interface slope diverging on the side of the drop. Thus the description of this part of the flow is beyond the capabilities of a slender-jet model. However, by keeping the full curvature term, we still hope to obtain a reasonable description of this transition region. At low values of De , the initial stages of the necking process at short times $t < De < 1$ are controlled by the linear stability of a viscoelastic fluid thread (Middleman (1965), Funada & Joseph (2003)); however ultimately at longer times $De < 1 < t$ there will still be a crossover to the exponential necking regime, provided the polymer chains are sufficiently extensible. We do not consider these regimes further in the present study.

Our paper is organised as follows: In the next section we develop and motivate the lubrication equations to be used for the remainder of this paper. A numerical simulation illustrates the regimes to be analysed below. The third section is devoted to the study of the neo-Hookean regime, where polymer relaxation can be neglected. First we derive a simplified, local description from the model equations. This local description is then used to compute the asymptotic thread radius, and to describe the propagation of elastic waves on the thread. The fourth section deals with the long time regime at finite De for which exponential thinning of threads is observed. After giving a qualitative description of the shape and flow inside the thread, we introduce a similarity description valid in the corner where a cylindrical thread meets a spherical drop. If De is large enough to make only elastic and surface contributions relevant, we can compute all but one of the free parameters of the solution. This last parameter, the thread radius, can be estimated by matching to the early-time regime. The numerical results are compared with experimental observations using a dilute solution of monodisperse polystyrene which is well-described by the Oldroyd-B constitutive model. Measurements of the evolution in the mid-filament radius and the evolution of the spatial profile of the filament are well-described by the theory. In the final section we discuss work that remains to be done within the framework of the present model, as well as perspectives for inclusion of other effects that lie beyond it.

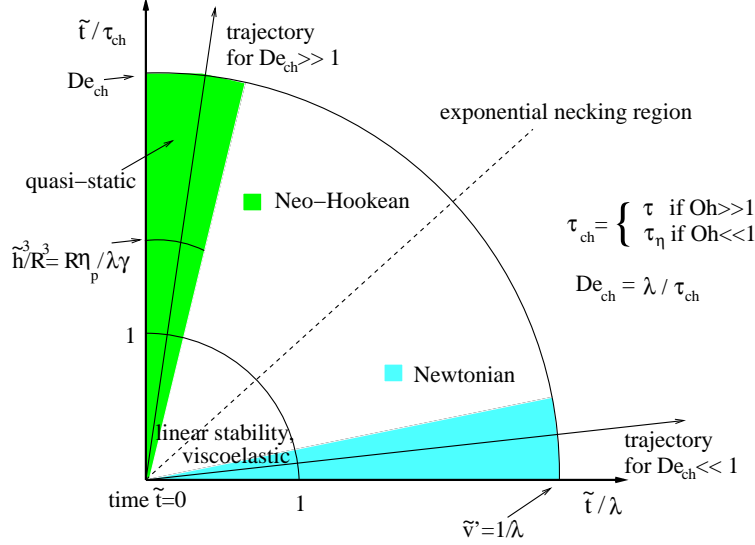


FIGURE 3. Schematic diagram showing the transient evolution of viscoelastic fluid threads. Trajectories correspond to rays of constant slope, given by the ‘intrinsic’ Deborah number $De = \lambda/\tau_{ch}$, where τ_{ch} is the characteristic capillary timescale (depending on whether viscous or inertial effects are more important in the bulk). The focus of this paper is on the sector corresponding to large slopes, and more details are given in the text. For small slopes the behaviour is Newtonian for a significant portion of the evolution, until the stretch rate \tilde{v}' exceeds the inverse polymer relaxation time.

2. Model and simulation

2.1. One-dimensional equations

In this paper we confine ourselves to the study of a simplified version of the Oldroyd B model for polymeric liquids, assuming that the radius $h(z, t)$ of the liquid column varies slowly. Thus the variation of hydrodynamic variables inside the column is also small, and we can confine ourselves to the leading order approximation in an expansion in the radius. For example, $v(z, t)$ below is the axial velocity at the centre of the jet. A derivation of the relevant equations has been given in Forest et al. (1990), so we just give the final result and briefly discuss its physical significance:

$$\frac{\partial h^2}{\partial t} + \frac{\partial}{\partial z} (vh^2) = 0 \quad (2.1)$$

$$\frac{\partial v}{\partial t} + v \frac{\partial v}{\partial z} = -\frac{\partial \kappa}{\partial z} + 3\nu_s \frac{1}{h^2} \frac{\partial}{\partial z} \left(h^2 \frac{\partial v}{\partial z} \right) + \frac{1}{h^2} \frac{\partial}{\partial z} (h^2 (\sigma_{zz} - \sigma_{rr})) \quad (2.2)$$

$$\frac{\partial \sigma_{zz}}{\partial t} + v \frac{\partial \sigma_{zz}}{\partial z} = 2 \frac{\partial v}{\partial z} \sigma_{zz} + 2 \frac{\nu_p}{De} \frac{\partial v}{\partial z} - \frac{\sigma_{zz}}{De} \quad (2.3)$$

$$\frac{\partial \sigma_{rr}}{\partial t} + v \frac{\partial \sigma_{rr}}{\partial z} = -\frac{\partial v}{\partial z} \sigma_{rr} - \frac{\nu_p}{De} \frac{\partial v}{\partial z} - \frac{\sigma_{rr}}{De} \quad (2.4)$$

Equation (2.1) expresses volume conservation, (2.2) is the momentum balance equation

in the one-dimensional approximation. The first term on the right of (2.2) is the gradient of the Laplace pressure, which is the main driving force. With the present scaling, the capillary pressure gradient is simply the gradient of the mean curvature κ , which for later convenience will also be written as

$$-\frac{\partial \kappa}{\partial z} = \frac{1}{h^2} \frac{\partial}{\partial z} \left(h^2 \left(\frac{h_{zz}}{(1+h_z^2)^{\frac{3}{2}}} + \frac{1}{h(1+h_z^2)^{\frac{1}{2}}} \right) \right) \equiv \frac{1}{h^2} \frac{\partial}{\partial z} (h^2 K\{h\}) . \quad (2.5)$$

The second term on the right of (2.2) is the Newtonian contribution to the viscosity, multiplied by the dimensionless viscosity ν_s of the solvent. Finally the last term is the polymeric contribution; σ_{zz} and σ_{rr} are the diagonal terms of the extra stress tensor. The other components of the polymeric stress tensor do not enter at leading order. Using (2.5), equation (2.2) can finally be rewritten such that the inertial terms on the left are balanced by gradients of the tension in the thread:

$$\frac{\partial v}{\partial t} + v \frac{\partial v}{\partial z} = \frac{1}{h^2} \frac{\partial}{\partial z} \left[h^2 \left(K + 3\nu_s \frac{\partial v}{\partial z} + \sigma_{zz} - \sigma_{rr} \right) \right] . \quad (2.6)$$

For very viscous fluids the inertial terms on the left are negligible, and the terms in parentheses equal a (generally time-dependent) constant. If velocity gradients $\partial v/\partial z$ are small, (2.3) and (2.4) describe an additional *Newtonian* contribution ν_p to the total steady-state shear viscosity $\nu = \nu_s + \nu_p$. The presence of polymers also results in fluid viscoelasticity and the polymeric stress in the fluid responds with a dimensionless time delay of De , which is represented by the relaxation terms σ_{ij}/De on the right of (2.3) and (2.4). Finally a crucial term for the physics of the following is the first term on the right of (2.3) and (2.4), which describes the interaction of the polymer with the flow. In an extensional flow $\partial v/\partial z$ is positive, so the stress in the axial direction grows as the dumbbells modeling the polymeric contribution to the stress are stretched, while it decays in the radial direction.

2.2. Beads on a string

We are now in a position to study the behaviour of the model for various initial conditions and to compare to experiment. First, we simulate the decay of a long, initially unstretched cylinder of fluid. For our simulations we have used a numerical code analogous to the one developed earlier by Eggers & Dupont (1994), Eggers (1997) for Newtonian flows. It is fully implicit and uses adaptive regridding of the numerical mesh to fully resolve the fine structure of the flow. This is crucial to be able to describe some of the last stages of thread formation to be investigated in detail in section 4. We found that the demands on the solution of the implicit equations are much greater than in the Newtonian case, owing to a larger range of time scales in the flow. In general, several iterations of a Newton scheme were necessary for convergence, and significant restrictions had to be put on the time step. To further test for possible problems inherent in our numerical scheme, Another *explicit* code was also developed independently. In addition, all fields were represented in a uniform grid, as opposed to the staggered grid of the implicit code. The explicit code performed quite well except for the highest viscosities, where the time step imposed by the Courant condition became prohibitively small. In all our tests, we found no significant disagreement between the results of the two codes, so below we will no longer specify which one was used to obtain a specific result.

Figures 4 and 5 give an idea of the typical behaviour of a liquid filament in the absence of gravity, described by (2.1-2.4). The parameters were chosen to be identical to those of Fig. 2 in Chang et al. (1999); that is in the present scaling, $\nu_s = 0.79$, $\nu_p = 2.37$, and $De = 94.9$, except that our initial perturbation is smaller. The periodic boundary condition is

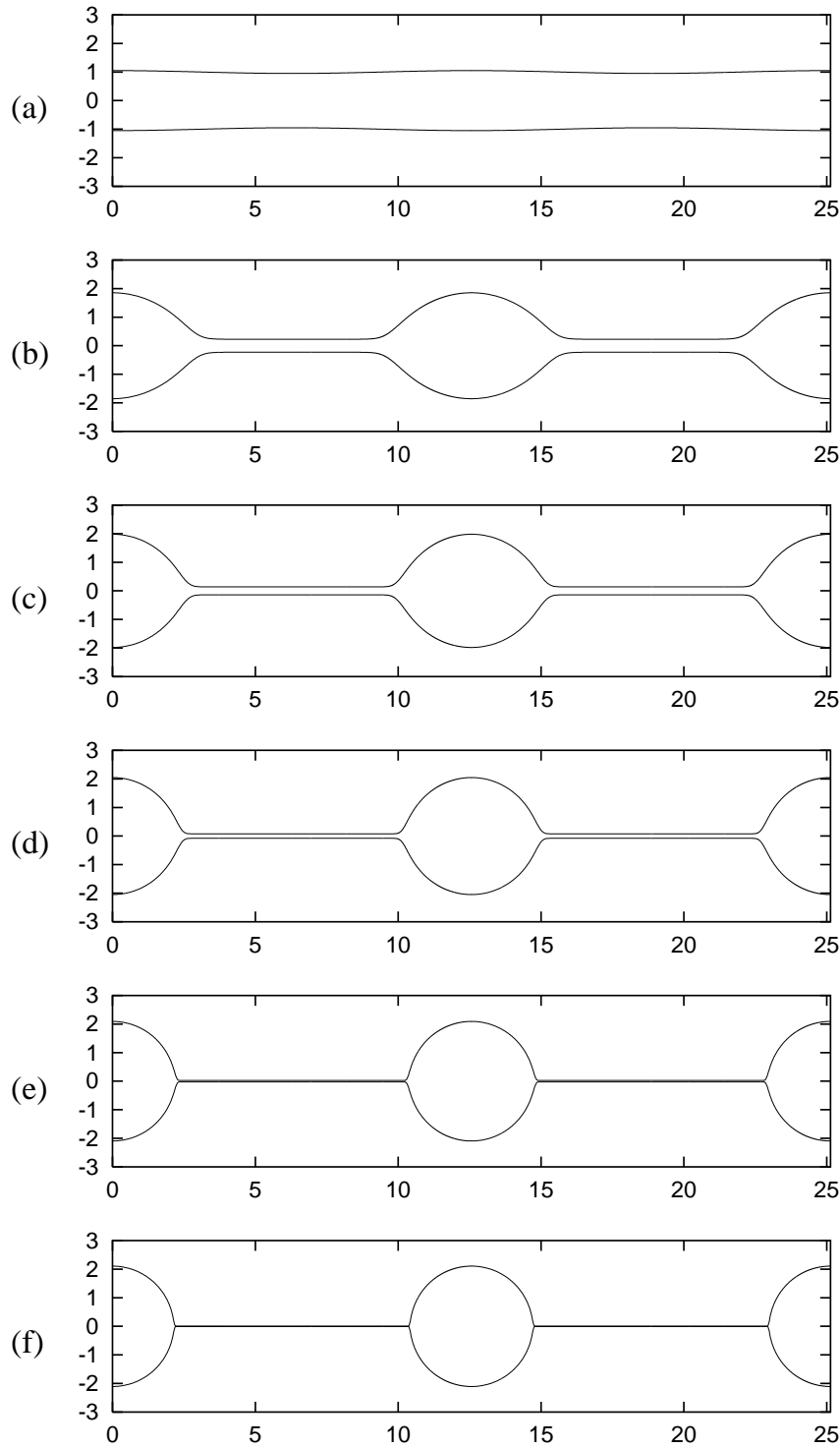


FIGURE 4. A typical series of profiles with periodic boundary conditions and period $L = 4\pi$. The dimensionless parameters are $\nu_s = 0.79$, $\nu_p = 2.37$, and $De = 94.9$. A very small sinusoidal perturbation was added in order to make the filament collapse. After the rapid formation of the beads-on-string structure, one observes the slow thinning of the thread. The relative dimensionless times of each profile are (a) 0.0, (b) 31.6, (c) 158.1, (d) 316.2, (e) 632.5 and (f) 948.7.

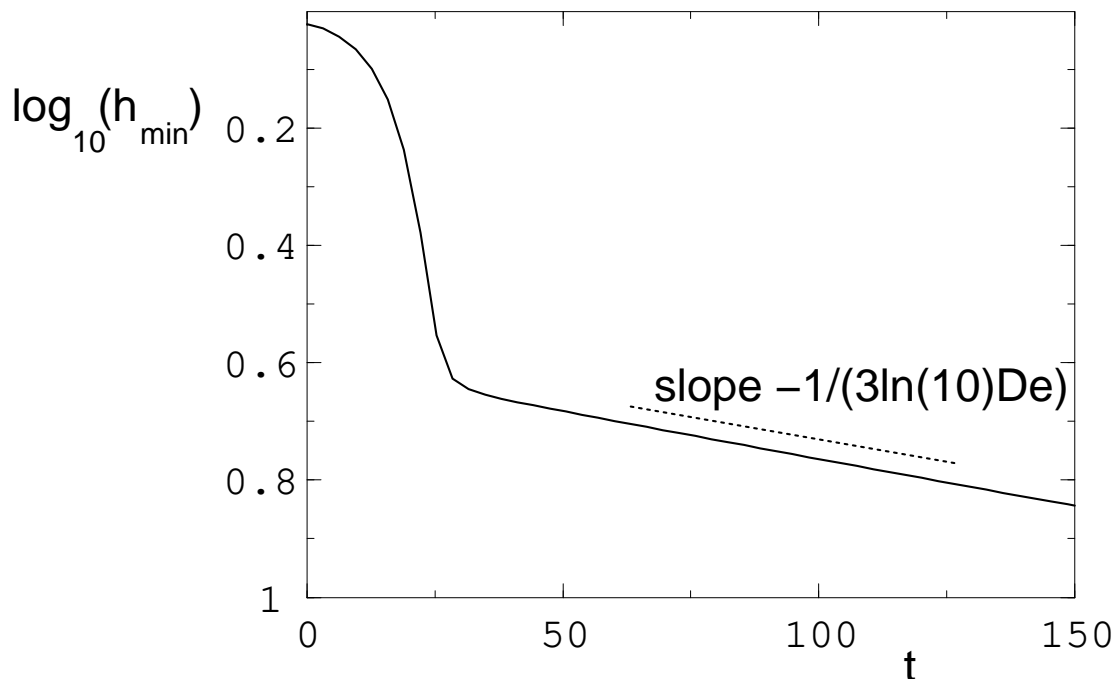


FIGURE 5. The minimum radius corresponding to the profiles shown in Fig.4. One clearly observes a rapid initial motion for times small compared to $De = 94.9$, followed by an exponential thinning at rate $1/(3De)$.

used here with the period $L = 4\pi$. The relaxation time scale for the polymer solute (λ) is approximately 95 times the capillary time scale, so at short times, viscoelastic relaxation effects can be neglected. Additionally, the Ohnesorge number is $Oh = \nu_s + \nu_p = 3.16$, so the flow is significantly damped by viscosity. Fig. 4 shows a sequence of profiles for a length of two periods (8π) at different times. After an initial period described by linear theory, a thin thread is formed between two round drops. The filament necks in the central region and the fluid expelled from this neck is accumulated in the two beads. The evolution in the minimum radius of the thread with time is shown in Fig. 5. There is an initial sharp decrease, until a sudden change in the slope occurs. This happens when the elastic stresses which build up in the deforming liquid bridge become dominant and a local elasto-capillary balance leads to the formation of a thin filament. The rest of the evolution consists of an exponential thinning of the filament, best seen in the logarithmic plot of Fig.5. The slope drawn into the figure corresponds to the theoretical prediction of section 4.

Structures very similar to Figure 4 are shown in the experiment of Figure 2 and have also been observed by Bazilevskii et al. (1981), Christanti & Walker (2001) for the decay of a liquid jet of polymer solution ejected from a nozzle. Good agreement with numerical simulations of one-dimensional models very similar to ours have been reported by Yarin (1993). However, it is very difficult in practice to produce liquid cylinders without stretching the polymers, since there is considerable shear inside the capillary tube and the nozzle. On the other hand, the shear flow inside the capillary is very difficult to model in the framework of the present one-dimensional description. Furthermore, each bead and ligament shown in Fig.2 corresponds to a ‘snapshot’ at a different elapsed convective time $\Delta\tilde{t} = L_{period}/v_{jet}$. Therefore, to compare quantitatively to experiments,

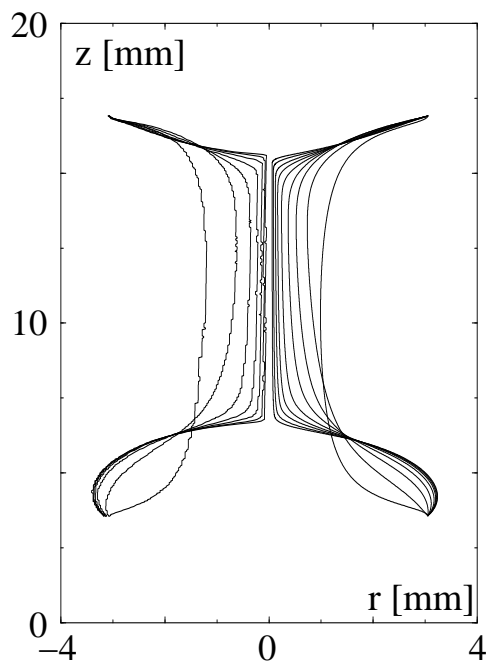


FIGURE 6. A comparison between experimental profiles (left), obtained from digitising the images of Fig. 1 and corresponding simulations (right), including the initial stretching and gravity (acting downward). The time difference between two consecutive images is 10 sec. The reduced variables corresponding to the experimental parameters are $\nu_s = 193.2$, $\nu_p = 29.04$, and $De = 296$. Note that there are *more* profiles from simulation to reach approximately the same thread radius, corresponding to a slight overestimation of the experimental time scale.

we prefer to use a setup that allows for a more quantitative description of the stretching history of the fluid column.

2.3. Liquid bridge

We now turn to the capillary thinning and breakup of a liquid bridge that has been subject to a very rapid initial stretching. During this extensional step strain process, which lasts 0.05 sec, hardly any polymer relaxation takes place, so the exact manner in which the plates are pulled apart is not very important. In fact, the initial stretching is well described by a simple model neglecting any spatial structure (Anna & McKinley (2001)). However, the simulation within the one-dimensional model is somewhat subtle, owing to a difficulty in imposing the boundary conditions at the end-plate. Namely, the no-slip boundary condition enforces a vanishing tangential velocity at the end-plate, and conse-

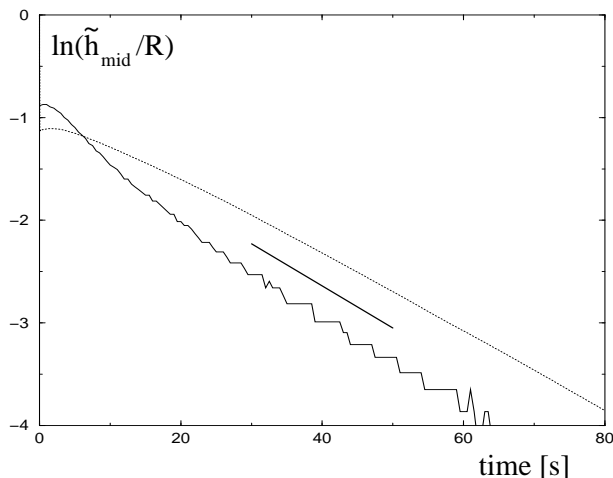


FIGURE 7. The logarithm of the normalised minimum radius corresponding to the experimental and theoretical profiles of Fig.6. The thick line is the theoretical prediction for the slope $-1/(3\lambda)$.

quently $\partial v/\partial z = 0$, while this is not true in the one-dimensional model. Since the stretch rate $\partial v/\partial z$ is in fact large over most of the bridge, this creates a thin boundary layer of the full three-dimensional flow near the end-plates. Failure to correctly implement this boundary layer leads to a detachment of the interface from the ends within the lubrication model. Following Stokes et al. (2000), we have avoided this problem by introducing a supplementary viscosity which strongly increases near the ends. This position-dependent viscosity has been constructed by matching to a three-dimensional squeeze flow near a solid wall. The effective “freezing” of the fluid prevents any lateral slip along the bounding wall.

Figures 6 and 7 allow for a direct comparison between simulation and experiment. The first digitised profile is taken just after cessation of stretching, after that a profile is shown every 10 sec. Theory and experiment show good agreement in all the basic features of the flow, such as the sagging under gravity and the formation of the thread. Two subtle differences can be seen: first, the timescale of the simulation is off by about 20%, so 9 experimental profiles are shown but only 7 theoretical ones, at which point about the same minimum thread radius is reached. This discrepancy, also seen in Figure 7, is quite acceptable considering that no adjustable parameters were introduced. Most of the difference stems from the early-time development, while the asymptotic slope of both simulation and experiment agrees well with the theoretical prediction.

The behaviour of h_{min} at early times is markedly different from that of a free jet, as discussed in detail in Anna & McKinley (2001). The rapid early decrease of h_{min} seen in Figure 5 is absent, since stresses are already large owing to the initial stretching of

the liquid bridge. On the contrary, some of this initial stress has to relax before further thinning can start, as seen in the plateau for the earliest times. Evidently there are some subtle features of the experimental relaxation processes which are not modelled correctly by our single-mode Oldroyd-B model. The initial stretch is also responsible for the absence of drops (“beads”) in the middle of the thread that formed on the free jet, cf. Figure 4. The reason is that the initial stretch is uniform, and this uniformity is conserved by the exponential stretching regime.

The second difference between the experimental and theoretical profiles of Figure 6 is that at the same minimum thread radius the corner between the thread and drops at the end is *sharper*. We will return to this when we discuss the structure of the corner region in detail in section 4.2.

3. Early time asymptotics

3.1. Local description

In this section we show that for early times $t \ll 1 \ll De$ the non-Newtonian contribution to the stress behaves like that of a neo-Hookean elastic solid, and can be expressed directly through the profile shape $h(z)$. This proves the phenomenological argument of Entov & Yarin (1984), in addition to identifying the correct value of the elastic modulus of the material:

$$G = \nu_p / De. \quad (3.1)$$

With the present scaling this is the same as the *elastocapillary* number introduced in Anna & McKinley (2001) and can also be written $G = Oh(1 - S)/De$. Following the procedure in Fontelos (2003) we rewrite (2.3),(2.4) in Lagrangian coordinates. This idea, introduced in Renardy (1994), is useful since the stretch of a fluid element can be written as $z_\alpha = 1/h^2$ (Renardy (1994), Eggers (1997)). This Lagrangian stretch $u \equiv z_\alpha$ is the derivative of the particle position z with respect to the label α of the particle in a reference configuration. Using the Lagrangian definition of the fluid velocity $z_t = v$ one finds that $v_z = u_t/u$ and thus

$$\sigma_{zz} + De \left(\frac{\partial \sigma_{zz}}{\partial t} - 2 \frac{u_t}{u} \sigma_{zz} \right) = 2\nu_p \frac{u_t}{u}, \quad (3.2)$$

$$\sigma_{rr} + De \left(\frac{\partial \sigma_{rr}}{\partial t} + \frac{u_t}{u} \sigma_{rr} \right) = -\nu_p \frac{u_t}{u}, \quad (3.3)$$

which can be rewritten as

$$e^{-\frac{t}{De}} \frac{\partial}{\partial t} \left(\frac{1}{u^2} e^{\frac{t}{De}} \sigma_{zz} \right) = 2G \frac{u_t}{u^3},$$

$$e^{-\frac{t}{De}} \frac{\partial}{\partial t} \left(u e^{\frac{t}{De}} \sigma_{rr} \right) = -G u_t.$$

If we assume that the initial stresses are zero (otherwise they remain as initial conditions) we can integrate the equations to find

$$\sigma_{zz} = 2Gu^2 e^{-\frac{t}{De}} \int_0^\tau e^{\frac{\tau}{De}} \frac{u_t}{u^3} d\tau = -Gu^2 e^{-\frac{t}{De}} \int_0^t e^{\frac{\tau}{De}} \left(\frac{1}{u^2} \right)_\tau d\tau,$$

$$\sigma_{rr} = -Gu^{-1} e^{-\frac{t}{De}} \int_0^t e^{\frac{\tau}{De}} u_\tau d\tau$$

Integration by parts yields

$$\sigma_{zz} = -G + G \frac{u^2}{u_0^2} e^{-\frac{t}{De}} + \frac{G}{De} u^2 e^{-\frac{t}{De}} \int_0^t e^{\frac{\tau}{De}} \frac{1}{u^2} d\tau, \quad (3.4)$$

$$\sigma_{rr} = -G + G \frac{u^{-1}}{u_0^{-1}} e^{-\frac{t}{De}} + \frac{G}{De} u^{-1} e^{-\frac{t}{De}} \int_0^t e^{\frac{\tau}{De}} u d\tau, \quad (3.5)$$

where the integrals are taken along Lagrangian paths, i.e. for constant particle label α . However, for $t \ll De$ the integral can be neglected relative to De and the exponential is close to unity. For the case that the initial deformation of the bridge is small, i.e. that u_0 is almost constant, (3.4,3.5) only contains Lagrangian labels at the same time t , which can simply be replaced by ordinary Eulerian coordinates by applying the inverse transformation. Remembering also that with the scalings used throughout this paper $u_0 = R_0 = 1$, we find

$$h^2 (\sigma_{zz} - \sigma_{rr}) = G (1/h^2 - h^4) + O(t/De). \quad (3.6)$$

This expression is the well-known result for the neo-Hookean rubber material if we recognize that the Lagrangian stretch is $u = 1/h^2$. Thus finally the equation for the velocity is

$$\frac{\partial v}{\partial t} + v \frac{\partial v}{\partial z} = \frac{1}{h^2} \frac{\partial}{\partial z} \left(h^2 K + 3\nu_s h^2 \frac{\partial v}{\partial z} + G (1/h^2 - h^4) \right), \quad (3.7)$$

where K is defined in (2.5). Of course, (3.7) can also be confirmed directly by applying the limit $t \ll 1 \ll De$ to the Eulerian equations (2.3,2.4), but it is hard to guess a priori without the use of Lagrangian coordinates.

As a numerical test of the quality of the local approximation, we performed two simulations similar to that of Fig. 4, but for two different *Deborah* numbers. Fig. 8 shows the evolution of the interface profile at different times for $De = 94.9$, $\nu_p = 2.37$ (left column), and $De = 9490$, $\nu_p = 237$ (right column). The full lines are the solution of equations (2.1-2.4), while the dashed ones were obtained by replacing (2.2) by (3.7). For the simulation corresponding to moderate Deborah number, the duration t is of same order of the relaxation time De . And as we expected, the solution of the full equations and the one of the local approximation differ for times $t > De$. On the other hand, for the case of large Deborah number, $t \ll De$, the agreement of the two solutions is excellent. Indeed, we can hardly distinguish the dashed lines from the full ones in the right column with our naked eyes.

Throughout the process of filament formation, we find almost perfect agreement with the local model provided $De \gg 1$. Thus the local approximation is an extremely useful tool to investigate the early-time dynamics $t < 1 < De$ and the formation of the basic beads-on-string structure. We will therefore study the stationary filament solutions of the local model in the following subsection. After the filament has formed, the neo-Hookean elastic response of the local model leads to a stationary profile, while the effects of fluid viscoelasticity captured by the full equations leads to the filament continuing to thin exponentially in time.

At low viscosities, $Oh < 1$, the initial evolution can be considerably more complicated, but is still fully described by the local equations if De is sufficiently large. This is due to inertial effects also being important, so as the thread is formed, fluid may rebound from the drops, and an additional ‘secondary’ drop forms in the middle of the filament. This is also seen in experimental observations of jet breakup (Christanti & Walker (2001)) and drop pinch-off (Cooper-White et al. (2002)). In addition, capillary waves may develop, which we describe in subsection 3.3.

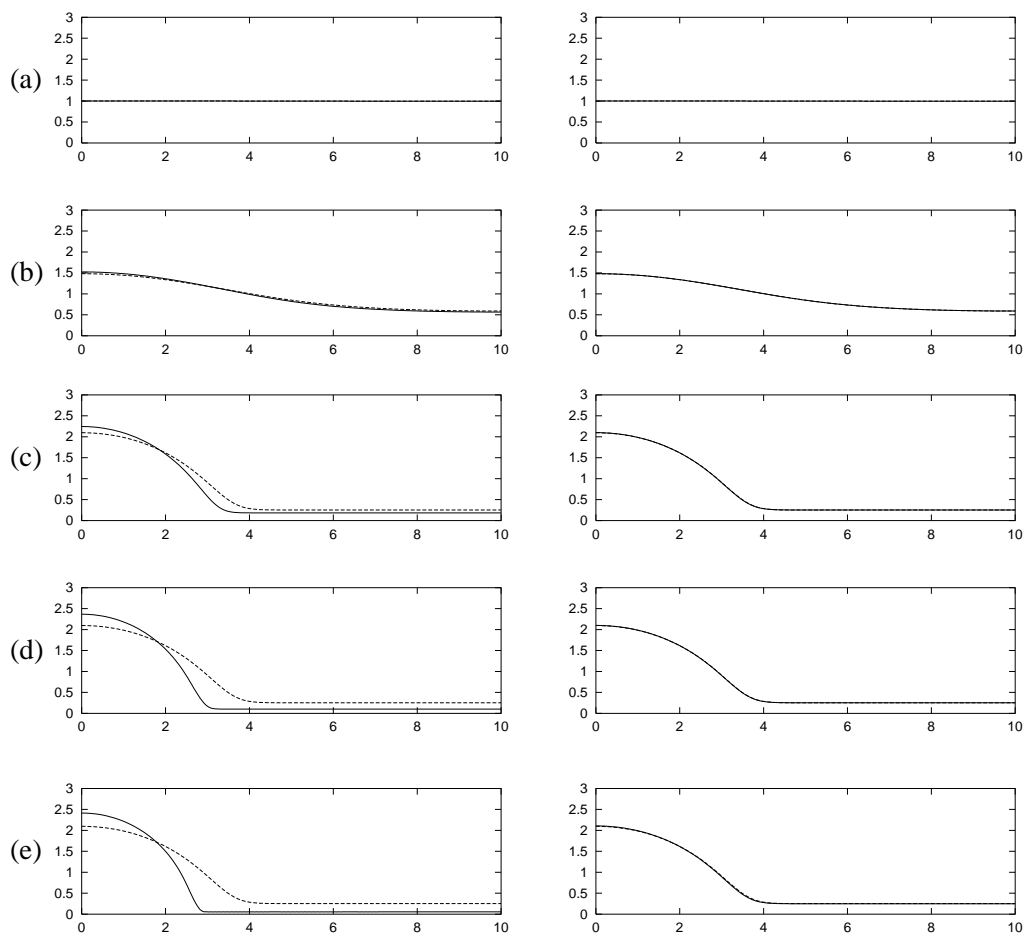


FIGURE 8. Comparison of interface profiles with period $L = 20$ and $\nu_s = 0.79$ between the full equations (full) and the local approximation (dashed lines): left column $De = 94.9$ and $\nu_p = 2.37$, and right column $De = 9490$ and $\nu_p = 237$. The relative times for each profile are (a) 31.6, (b) 79.1, (c) 158.1, (d) 316.2 and (e) 474.3. Evidently, for $t \ll De$ the agreement is excellent (right column).

3.2. Static solutions

In the neo-Hookean limit considered here, $De \rightarrow \infty$, the elastic stresses never relax, so at long times $t \gg De \gg 1$, surface tension is balanced by permanent elastic stresses to form a stationary solution, which obeys the equation

$$h^2 K + G(1/h^2 - h^4) = C, \quad (3.8)$$

which comes from integrating (3.7) once while dropping inertial terms. Apart from the appropriate boundary conditions on h , (3.8) has to be solved with the constraint of volume conservation

$$\pi \int_0^L h^2 = V, \quad (3.9)$$

which is needed to find all the constants of integration as well as C .

In particular, (3.8) allows for solutions with constant h

$$h + G(1/h^2 - h^4) = C, \quad (3.10)$$

where we have assumed a constant initial height $h_0 = 1$. The solutions of equation (3.10) correspond to the thin cylindrical threads of constant radius described earlier. To determine their radius, one needs the value of the constant C , which only follows from a solution of the full system (3.8) with proper constraint (3.9). Entov & Yarin (1984) have described a procedure which matches solutions of (3.10) to almost circular drops in the limit of small elastic modulus G , from which the thread radius can be determined analytically. Below we will reproduce their calculation, which will turn out to be relevant for the calculation of thread thinning as well.

First, in the drop region the radius h is of order one and one can neglect the terms multiplied by G in the limit we are interested in. Thus one is left with the contribution from surface tension alone, and the solution is a spherical drop,

$$h(z) = R\sqrt{1 - (1 + z/R)^2}. \quad (3.11)$$

Here R is the radius of the drop, which is set by the volume constraint (3.9), and must be a quantity of order one. The other constant of integration was used to place the edge of the drop, which merges onto the thread, at the origin. In the following we will assume that the filament is to the right of the drop, in the region of positive z , while the matching takes place in the neighbourhood of the origin.

To match the drop (3.11) onto a constant solution, we have to analyse (3.8) in the limit $G \rightarrow 0$, guessing that in the crossover region h is still small. Thus h^4 can be neglected relative to $1/h^2$ and we can eliminate the elastic modulus from the equation with the scaling

$$h = G^{1/3}H, \quad z = G^{1/3}Z, \quad C = G^{1/3}C_1, \quad (3.12)$$

where now all rescaled quantities are of order unity and H obeys the equation

$$H^2 K\{H\} + 1/H^2 = C_1. \quad (3.13)$$

Denoting derivatives with respect to X by primes and multiplying (3.13) by H'/H^3 one finds the following first integral,

$$H' = - \left[\frac{4H^2}{(C_1 + 2H^2/R_1 - 1/(2H^2))^2} - 1 \right]^{1/2}, \quad (3.14)$$

where R_1 is a constant of integration. Here we have used

$$\left(\frac{1}{H^2 \sqrt{1 + H_z^2}} \right)' = - \frac{H_z}{H \sqrt{1 + H_z^2}} - \frac{H_z H_{zz}}{H \sqrt{(1 + H_z^2)^3}}.$$

The constant C_1 and R_1 in the equation (3.14) have to be chosen so that the solution matches both the drop and the thread.

We begin with the matching to the drop for $z < 0$. For large R_1 there is region with

$$R_1^{1/2} \ll H \ll R_1 \quad (3.15)$$

in which (3.14) is approximated by

$$H' \approx -R_1/H$$

with solution $H = \sqrt{2R_1|z|}$. By comparing with the expansion of the drop profile (3.11)

for small $|z|$ we find

$$R_1 = R/G^{1/3}, \quad (3.16)$$

so R_1 is indeed large for small $\bar{\nu}$. In terms of the variable z , the matching region (3.15) is defined by

$$1 \ll |z| \ll R_1. \quad (3.17)$$

On the other (thread) side of the problem ($z > 0$) the slope has to go to zero and thus

$$C_1 + 2H_0^2/R_1^2 - 1/(2H_0^2) = 2H_0,$$

giving C_1 in terms of H_0 . To finally find H_0 , one has to make sure that small perturbations around the constant solution do not grow. Putting $H = H_0(1 + \delta)$, we find

$$\delta' \sim [(1 - 2H_0/R_1 - 1/(2H_0^2))\delta + O(\delta^2)]^{1/2}.$$

For δ not to grow the expression in parentheses must vanish, and since R_1 becomes large in the limit $G \rightarrow 0$, we are finally left with $H_0 = 1/2^{1/3}$ and $C_1 = 3/2^{1/3}$. Thus the central result of our analysis is that the thickness of the thread becomes

$$h_{thread} = \left(\frac{G}{2}\right)^{1/3}. \quad (3.18)$$

For the parameters of Fig. 8 we find $h_{thread} = 0.232$ from (3.18), to be compared with the observed value of $h_{min} = 0.253$. The quality of the approximation quickly improves as the scale separation between thread thickness and drop size becomes even more complete.

3.3. Linear stability

The analyses of the previous two subsections can be used to perform a linear stability analysis of the stationary threads that form in the limit of very large De . This will be a good approximation on time scales much smaller than $t < 1 \ll De$, over which the thread maintains an almost uniform axial profile. This is a relatively simple calculation to do, since the base solution is constant in both space and time. Thus we put

$$h = h_0 + \tilde{h}, \quad v = \tilde{v}, \quad (3.19)$$

where h_0 is constant and \tilde{h} , \tilde{v} are small perturbations around the base solution. Then the linearised equations turn out to be:

$$\begin{aligned} \frac{\partial \tilde{h}}{\partial t} + \frac{1}{2}h_0 \frac{\partial \tilde{v}}{\partial z} &= 0 \\ \frac{\partial \tilde{v}}{\partial t} &= \frac{1}{h_0^2} \frac{\partial}{\partial z} \left(h_0^2 \tilde{h}_{zz} + 3\nu_s h_0^2 \frac{\partial \tilde{v}}{\partial z} + \left(1 - \frac{2}{h_0^3}G - 4h_0^3G\right) \tilde{h} \right), \end{aligned}$$

which can be combined to the following equation for \tilde{h} alone:

$$\frac{\partial^2 \tilde{h}}{\partial t^2} = -\frac{1}{2}h_0 \frac{\partial^4 \tilde{h}}{\partial z^4} + 3h_0\nu_s \frac{\partial^3 \tilde{h}}{\partial z^2 \partial t} - \frac{1}{2h_0} \left(1 - \frac{2}{h_0^3}G - 4h_0^3G\right) \frac{\partial^2 \tilde{h}}{\partial z^2}. \quad (3.20)$$

Using a wave ansatz of the form $\tilde{h}(z, t) = \epsilon \exp i(kz - \omega t)$ we find the dispersion relation

$$\omega^2 = -\frac{k^2}{2h_0}(1 - h_0^2 k^2) + \frac{k^2 G}{h_0^4}(1 + 2h_0^6) + 3i\nu_s h_0 \omega k^2. \quad (3.21)$$

The first term on the right comes from surface tension and describes the usual Rayleigh-Plateau instability of a Newtonian liquid jet. If we disregard the polymer contribution

we find complex ω for $kh_0 < 1$ and thus exponential growth of perturbations. The presence of elastic stresses shifts the critical value of k to slightly smaller values of k , thus stabilising the flow. If however this critical value as well as the maximum growth rate are compared to a Newtonian fluid with the same zero shear rate viscosity η_0 , one finds that the instability grows *faster* (e.g. Middleman (1965), Goldin et al. (1969), Chang et al. (1999)).

In the thin thread region described by (3.18), on the other hand, one is effectively dealing with an elastic medium and can see the propagation of elastic waves. Only taking into account the elastic contributions one finds

$$\omega = \pm \left[\frac{\bar{\nu}k^2}{h_0^4} - (3\nu_s h_0 k^2 / 2)^2 \right]^{1/2} + 3i\nu_s h_0 k / 2. \quad (3.22)$$

Hence for small viscosities there is little damping and waves are very easily excited on the threads, which causes considerable numerical problems to properly resolve them. In the limit of zero viscosity the elastic wave speed is given by

$$v_{el} = \frac{\sqrt{G}}{h_0^2}. \quad (3.23)$$

4. Late time asymptotics

4.1. Thread thinning

The formation of threads described in the previous section is a result of the interplay of surface tension and elastic forces. Any additional thinning of the thread results in an extensional flow, resisted by further stretching of the polymers. On times longer than De however the stress gradually relaxes, and the thread thins at an exponential rate β . This rate is easily determined from a balance of surface tension and elastic forces in (2.2), assuming a spatially constant profile (e.g. Bazilevskii et al. (1981), Renardy (1995), Entov & Hinch (1997))

$$h(z, t) = h_0 \exp(-\beta t). \quad (4.1)$$

From volume conservation (2.1) one finds that the extension rate $\partial_z v = 2\beta$ in the thread is constant. The exponential growth of the axial stress σ_{zz} is described by (2.3), and assuming a spatially constant σ_{zz} one immediately finds

$$\sigma_{zz}(z, t) = \sigma_0 \exp[(4\beta - De)t]. \quad (4.2)$$

The radial stress σ_{rr} *decreases* exponentially and does not figure in the balance. Remembering that capillary pressure is balanced with σ_{zz} in (2.2) and rewriting the pressure gradient according to (2.5) one finds

$$h + h^2 \sigma_{zz} = C, \quad (4.3)$$

performing one spatial integration. For the balance (4.3) to be consistent σ_{zz} must grow like $1/h$, and thus $\beta = 1/(3De)$, implying that the constant of integration C itself decays like

$$C = a_1 \exp[-t/3De]. \quad (4.4)$$

This means that the thinning rate of the thread is directly related to the time scale of the polymer, providing for a convenient experimental probe.

To obtain a clearer physical picture, we plot in Figure 9 the thread radius, normalised

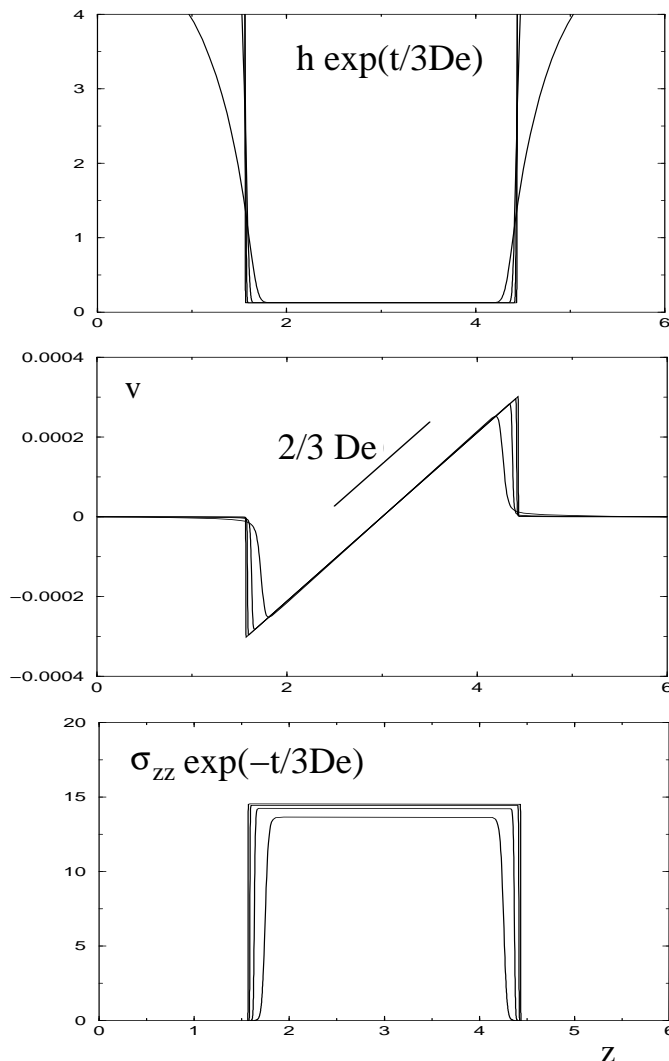


FIGURE 9. Profiles of the radius, the velocity, and the axial stress, normalised by their values in the thread, in the regime of exponential thinning. The parameters are $De = 3164$ and $\nu_s = \nu_p = 95.6$. The extension rate inside the thread is $2/(3De)$.

by the exponential factor $\ell = \exp[-t/3De]$, the velocity in the thread, and $\ell\sigma_{zz}$ for a number of different times during the thinning. As predicted, $h(z)$ and $\sigma(z)$ are very nearly constant over the thread, and they collapse nicely as anticipated by the above scaling laws. Furthermore, the extension rate $\partial_z v$ has the constant positive value 2β inside the thread, expressing the fact that fluid is expelled from it. In response, the stress σ_{zz} grows to large *positive* values, so both contributions on the left-hand side of (4.3) are always positive. This means that the constant of integration in (4.3) (which below we will compute explicitly in the limit of large De) has to be kept for a consistent balance and is needed to determine the stress and thus the extensional viscosity from a measurement of the thread radius. For large De this makes the stress twice as large (apart from a difference in sign) as determined from the customary direct balance between capillary and elastic stresses (e.g. Bazilevskii et al. (1981), Entov & Hinch (1997), Anna & McKinley (2001)).

Since the total length L of the thread is a constant quantity, the maximum value of the velocity

$$v_{max} \approx \frac{L}{3De} \quad (4.5)$$

behaves like the inverse of the Deborah number, and is thus small in the limit that is the chief focus of this paper. A number of experiments (e.g. Bazilevsky et al. (1997), Anna & McKinley (2001)) have confirmed the prediction (4.1). In particular in Anna & McKinley (2001) the relaxation time was determined independently, and the thinning rate was found to conform with the prediction $\beta = 1/(3De)$. At both ends of the thread, the velocity and the stress fall to zero very sharply, and the profile merges onto a static drop with radius R . Next we will focus on this transition region, whose scale is set by $\ell = \exp(-t/3De)$.

4.2. The corner region

According to the scalings found in the previous subsection, which implies the existence of a small length scale $\ell = \exp(-t/3De)$, it is natural to look for solutions of (2.1-2.2) of the form

$$\begin{aligned} h(z, t) &= \ell \bar{h}(\bar{z}, t) \\ v(z, t) &= \bar{v}(\bar{z}, t) \\ \sigma_{zz}(z, t) &= \ell^{-1} \bar{\sigma}_{zz}(\bar{z}, t), \end{aligned} \quad (4.6)$$

where $\bar{z} = \ell^{-1}(z - z_0)$. The origin z_0 must asymptotically lie in the similarity region. A convenient choice is the position of the extremum of the velocity in the limit $\ell \rightarrow 0$. Since σ_{rr} is exponentially small inside the thread, it can be left out of our analysis. Thus the equations for \bar{h} , \bar{v} , and $\bar{\sigma}_{zz}$ are

$$\begin{aligned} 2\ell \dot{\bar{h}}\bar{h} - \frac{2\ell}{3De} (\bar{h}^2 - \bar{z}\bar{h}\bar{h}') + [\bar{v}\bar{h}^2]' &= 0 \\ \bar{h}^2 \left(\ell^2 \dot{\bar{v}} + \frac{\ell^2 \bar{z}}{3De} \bar{v}' + \ell \bar{v}\bar{v}' \right) &= [\bar{h}^2 K\{\bar{h}\} + \bar{h}^2 (3\nu_s \bar{v}' + \bar{\sigma}_{zz})]' \\ \ell \dot{\bar{\sigma}}_{zz} + \frac{\ell}{3De} (\bar{\sigma}_{zz} + \bar{z}\bar{\sigma}'_{zz}) + \bar{v}^3 \left[\frac{\bar{\sigma}_{zz}}{\bar{v}^2} \right]' &= \frac{\ell}{De} (2\nu_p \bar{v}' - \bar{\sigma}_{zz}), \end{aligned} \quad (4.7)$$

where the prime refers to differentiation with respect to the similarity variable \bar{z} and the overdot indicates differentiation with respect to time. Towards the thread our scaling ensures that \bar{h} , \bar{v} , and $\bar{\sigma}_{zz}$ tend toward the constants h_0 , v_0 , and σ_0 , respectively, as $\bar{z} \rightarrow \infty$. (Without loss of generality, we assume that the thread is to the right of the transition region.) The length scale ℓ becomes exponentially small for $t \rightarrow \infty$ and for any finite \bar{z} , terms proportional to ℓ or ℓ^2 may be dropped. Looking for time-independent solutions of (4.7) and integrating once, we find

$$\begin{aligned} \bar{v}\bar{h}^2 &= v_0 h_0^2 \\ \bar{h}^2 K\{\bar{h}\} + \bar{h}^2 (3\nu_s \bar{v}' + \bar{\sigma}_{zz}) &= h_0 + h_0^2 \sigma_0 \\ \bar{\sigma}_{zz}/\bar{v}^2 &= \sigma_0/v_0^2. \end{aligned} \quad (4.8)$$

Eliminating \bar{v} and $\bar{\sigma}_{zz}$, we end up with

$$\bar{h}^2 K\{\bar{h}\} + \bar{h}^2 (-a_2 \bar{h}'/\bar{h}^3 + a_3/\bar{h}^4) = a_1, \quad (4.9)$$

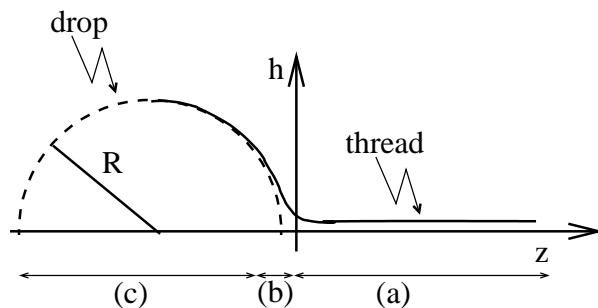


FIGURE 10. A schematic of the different regions near the corner.

where $a_1 = h_0 + h_0^2 \sigma_0$, $a_2 = 6\nu_s v_0 h_0^2$, and $a_3 = \sigma_0 h_0^4$. In general, equation (4.9) is no longer valid inside the drop, because here the profile $h(z, t)$ is almost stationary, thus \bar{h} varies like ℓ^{-1} , implying that the time derivative $\dot{\bar{h}}$ is proportional to $1/(\ell De)$. In addition, the similarity variable \bar{z} is also of order $1/\ell$ inside the drop. Therefore we have to distinguish three different regions, as shown in schematically in Figure 10.

(a) The similarity region near the thread described by (4.9).
 (c) The solution inside the almost spherical drop, where the velocity and stress fields relax towards zero.

(b) A transition region connecting the dynamical region (a) with the static region (c).

However in the limit of large De which is the main focus of this paper, velocities are of the order of $1/De$, and the contribution $-a_2 \bar{h}' / \bar{h}$ in (4.9), which comes from the viscous stress, can be neglected. The same is true for the left hand side of the second equation (4.7), as we will show in more detail in the appendix. Physically this limit corresponds to a situation where the fluid flow becomes irrelevant to the problem, which is dominated by surface tension and elastic contributions. Since the solution of (4.9) matches onto the drop, \bar{h} must become as large as desired for a sufficiently large \bar{z} . But this means that the contribution from $\bar{h}^{-2} \bar{\sigma}_{zz} = a_3 / \bar{h}^2$ is negligible compared to the constant a_1 outside of the similarity region. Thus although $\bar{\sigma}_{zz}$ can no longer be written as a simple function of \bar{h} in regions (b) and (c), it does not contribute to leading order outside of the similarity region (a). In summary, this implies that (4.9) with $a_2 = 0$ is valid *everywhere* in regions (a)-(c).

The constant a_3 can be scaled out by putting

$$\bar{h}(\bar{z}, t) = a_3^{1/3} g(\zeta \equiv \bar{z}/a_3^{1/3}, t), \quad (4.10)$$

and so we finally find

$$g^2 K\{g\} + 1/g^2 = C_1 \quad (4.11)$$

where $C_1 = a_1/a_3^{1/3}$.

Equation (4.11) is identical to (3.13), describing the stationary thread in the local approximation. The matching described in section 3.2

can thus be applied with very slight modifications. Multiplying (4.11) by the integrating factor g'/g^3 and integrating once, we obtain

$$g' = - \left[\frac{4g^2}{(C_1 + 2g^2/R_1(t) - 1/(2g^2))^2} - 1 \right]^{1/2}. \quad (4.12)$$

We seek values of C_1 and $R_1(t)$ such that

$$g(\zeta, t) \sim \text{Const.} \quad \text{when } \zeta \gg 1, \quad (4.13)$$

$$g(\zeta, t) \sim (2R)^{\frac{1}{2}} (-\ell^{-1} a_3^{-1/3} \zeta)^{\frac{1}{2}} \quad \text{when } \zeta \ll -1, \quad (4.14)$$

implying matching with the filament and the drop respectively. In order to match to the stationary drop of radius R we put $R_1(t) = R/(\ell a_3^{1/3})$ in analogy to (3.16), and in the limit of $t \rightarrow \infty$ we arrive at the equation

$$g' = - \left[\frac{4g^2}{(C_1 - 1/(2g^2))^2} - 1 \right]^{1/2}. \quad (4.15)$$

The procedure to match with the filament described in section 3.2 establishes that $C_1 = 3/2^{1/3}$ and

$$\sigma_0 = 2/h_0, \quad a_1 = 3h_0. \quad (4.16)$$

The transition region (b) between the drop and the thread is by virtue of (3.17) defined by

$$1 \ll |\bar{z}| \ll R/\ell. \quad (4.17)$$

In this region the solution is

$$g = \sqrt{2R_1|\bar{z}|}, \quad (4.18)$$

which in physical variables reads $h = \sqrt{2R|\bar{z}|}$ and thus matches to the stationary drop. The readily measurable amplitude h_0 of the thread thinning rate remains the only free parameter of the theory. Remarkably, the amplitude of the stress is exactly *twice* the value expected from a naive balance of capillary and elastic forces.

Integrating (4.15) with initial radius $1/2^{1/3}$ given by the form of the solution (4.15) (plus an arbitrarily small perturbation) one finds the universal profile shape g . The similarity profile \bar{h} is then given by (4.10) with $a_3 = 2h_0^3$. From Figure 9 one reads off that $h_0 = 0.1275$ for our simulation with $De = 3164 \gg 1$, and the numerically computed profiles in the corner region can easily be converted to give the rescaled profile $g(\zeta)$. The similarity profiles, computed from the numerical results of Figure 9 for four different times (solid lines), are compared with the theoretical prediction (dotted line) in Figure 11. As t grows, the rescaled profiles converge nicely to the theoretical prediction.

Finally, we compare our theoretical results to experiments. To that end, high resolution images of experimental profiles were taken by focusing a video microscope on the corner region.

Figure 12 shows a sequence of digitized images of the upper corner, which becomes increasingly sharp as the thread thins. To test our similarity theory, the profiles corresponding to the latest stages of pinching were rescaled using the minimum thread radius for both axes. As shown in Figure 13, the experimental profiles converge nicely onto a master curve, in very much the same way as the computed profiles of Figure 11 do. However, the experimental profiles turn out to be *sharper* than theory predicts. Thus the

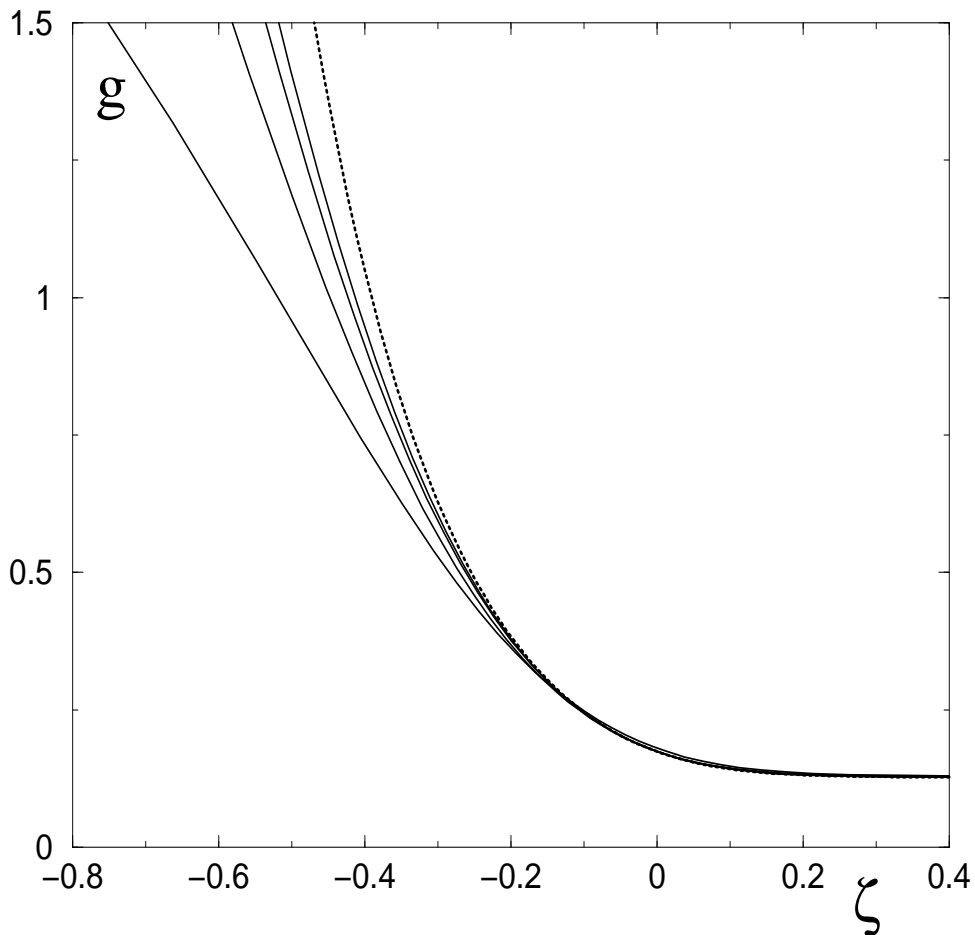


FIGURE 11. A comparison of our similarity theory for large De (dashed line) with rescaled profiles from a numerical simulation with parameters as in Figure 9, at $\log_{10}(h_{min}) = -1.5, -2, -2.5,$ and -3 . The dashed line was obtained from integrating (4.15), and rescaling according to (4.10), with $\zeta = \bar{z}/a_3^{1/3}$.

asymptotic result given by theory needs to be shrunk horizontally by a factor of 0.5 to fit the experimental curves. The resulting curve is given as the dotted line in Figure 13.

The constant h_0 is the only remaining adjustable parameter for the description of the corner region. In the case of the free jet, cf. section 2.2, it can in fact also be estimated in the limit that the relaxation time De of the polymer is much larger than the time t_{fil} needed to form the primary filament. Namely, equating the thread thickness (3.18) given by the local theory of section 3 with $h_{min} = h_0 \exp(-t_{fil}/3De)$ one finds

$$h_0 = \exp(t_{fil}/(3De)) \left(\frac{G}{2}\right)^{1/3}.$$

Thus in the limit that De is much larger than t_{fil} one simply has

$$h_{min}(t) = \left(\frac{G}{2}\right)^{1/3} \exp(-t/3De), \quad (4.19)$$

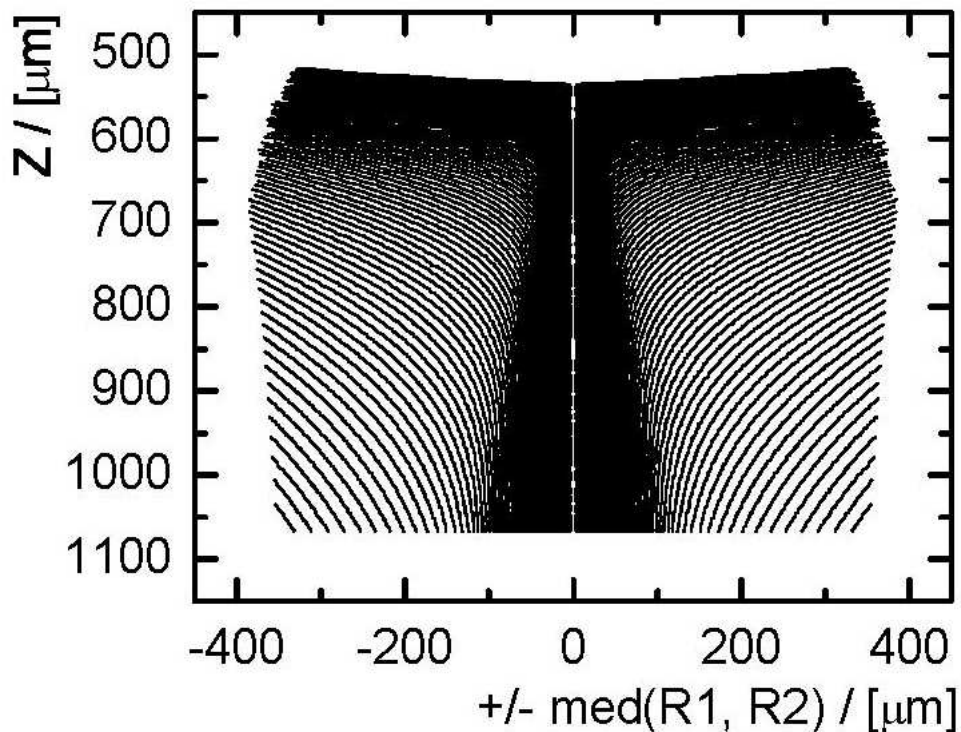


FIGURE 12. An experimental closeup of the upper corner of the liquid bridge. Shown is the same experiment as Figure 1, but under a microscope. The time interval between two consecutive profiles is 0.5 sec.

which is smaller by a factor of $2^{-1/3}$ than the result given in Bazilevsky et al. (1997) and Entov & Hinch (1997), based on a direct balance of elastic and surface tension forces. Fitting a straight line to the exponential thinning regime of Figure 5, we obtain $h_0 = 0.247$, in excellent agreement with the theoretical prediction of (4.19), $h_0 = (G/2)^{1/3} = 0.232$.

5. Discussion

In the present paper, confining ourselves to the simplest possible model for a dilute polymer solution, we have reached a rather complete description of the formation and subsequent development of the beads-on-string structure. Some details, of course, remain to be elaborated.

At low viscosities or high surface tension, $Oh \ll 1 \ll De$ our preliminary studies (e.g. Li & Fontelos (2003)) indicate that a complex succession of beads may be generated owing to inertial effects. Namely, fluid that rebounds from one of the large drops leads to capillary waves that travel on the thread, and can form one or more additional drops. After a sequence of drops has formed, these drops are subject to possible merging, or draining processes.

A similar phenomenon of secondary drop formation has been described in Chang et al. (1999) and is referred to as ‘recoil’. This recoil leads to the formation of a secondary filament between the secondary and main drops which, as claimed in Chang et al. (1999),

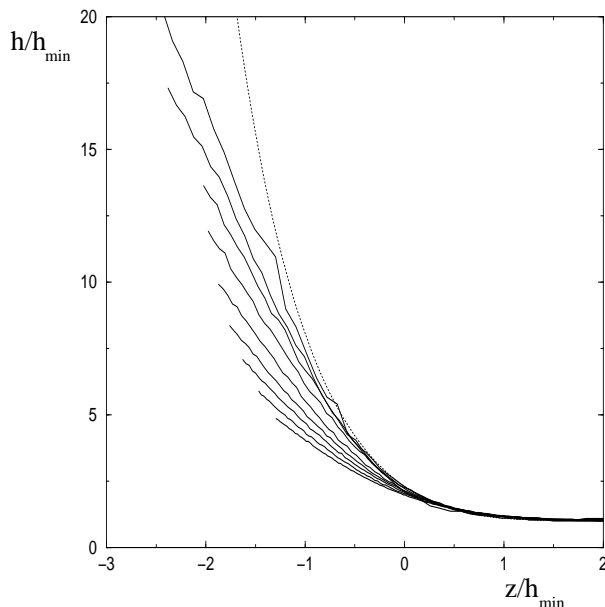


FIGURE 13. The last 9 profiles of Figure 12, with both axes rescaled by the minimum thread radius. The dotted line corresponds to the asymptotic theory also shown in Figure 11, but with the horizontal axis *shrunk* by a factor of 0.5.

exhibits a series of subsequent instabilities. However, for the parameters given in Chang et al. (1999) we found no indication for the formation of a secondary filament, but only for significantly lower viscosity or higher surface tension. Even if we do find a secondary filament, its presence is due to inertia, while Chang et al. (1999) claim their instability to be independent of inertial effects. Never did we find any indication of another instability leading to a third generation filament. These observations have been checked using both our implicit and explicit codes, making sure that the resolution was sufficient in the thin transition region between filament and drop. Insufficient resolution could occasionally lead to instabilities that vanished as resolution was increased.

Still within the framework of the Oldroyd-B model, but at more moderate values of $De \sim O(1)$, viscous flow effects would have to be taken into account (cf. Fig.3). As indicated above, the velocity in the corner region is proportional to $1/De$, thus in the limit of large De , viscous effects drop out and only capillary and elastic forces remain. In the presence of viscous forces, equation (4.9) can be applied for any finite value of the similarity variable \bar{z} . However, we have not yet succeeded in matching the solution described by (4.9) with the stationary drop in the general case. The reason is that whilst in the similarity region close to the corner (between the thread and the drop) everything can be described by the thread profile \bar{h} alone, this is no longer possible in the transition region towards the stationary drop. Instead, the coupled system involving the drop shape, the velocity field, and the stress has to be treated. Indeed, even in the limit of large De where matching can be achieved using h alone, analytical computation of v and σ_{zz} is far from trivial (Fontelos (2002)).

A result of the present similarity description is that for very long times the drop develops into a perfect sphere, while the thread radius shrinks to zero. This means the profile at the point where the thread meets the drop develops into a right angle. The same conclusion, but using a completely different approach without making use of the

self-similar structure of the equations, was reached in Renardy (1994). The series of experimental profiles shown in Fig.12 supports this conclusion.

Unfortunately, the fact that the slope of the profile becomes increasingly large in the corner means that the lubrication equations, used throughout this paper, are no longer valid. While it does not seem likely that this fact changes the scaling found in the present paper, it is clear that the precise shape of the profile will be somewhat different for the full equations. Full numerical simulations will also be quite challenging to perform with the accuracy required to resolve the corner region in the presence of strong elastic effects. However, one could use the self-similar scaling proposed in the present paper to reduce the dynamical 3-D equations to a time-independent equation, analogous to (4.8). In rescaled coordinates, the scale of the corner is of order one, and a solution of the problem could be attempted numerically. For the near future, the most promising prospect appears to be to compare with experiments with very long, well characterised polymer solutions. Note that even within a full 3-D theory, the correct minimum radius cannot be obtained from a direct balance of elastic and surface tension forces, as it was done in earlier works (Entov & Hinch (1997), Bazilevsky et al. (1997)). The reason is that both contributions have the same sign (compare (4.3)), and thus cannot possibly balance. Instead, a matching to the drop has to be performed in order to determine the total tension in the thread.

Finally, there are myriad effects associated with departures from the Oldroyd-B model, some of which have already been incorporated into the description of thread thinning. For example, even a perfectly mono-disperse polymer solution is expected to be described by a *spectrum* of time scales, inherent in the complex relaxation dynamics of even a single polymer strand (deGennes (1979)). This is not expected to be a major limitation for the present theory, however. Bead-spring models of dilute polymer solutions indicate that there is a simple recursion formula relating the longest relaxation time λ and higher order relaxation processes, of the form $\lambda_k = \lambda/k^m$, with $m = 1.5, 2$ for the Zimm or Rouse models respectively (Bird et al. (1987)). The local rate of stretching in the cylindrical thread arising from the elastocapillary balance is sufficiently weak (in dimensional form $\dot{\epsilon} = 2/(3\lambda)$), that all other modal contributions to the stress (of the form of eqs. 2.3, 2.4) will decay away and not contribute to the elastic stress since the convective terms will be of the form $(2De)v'/k^m < 1$. A detailed analysis of the effect of such a spectrum of relaxation times was carried out in Entov & Hinch (1997), but using an incorrect form of the force balance, eq. (4.3).

The effect of the finite extensibility of a polymer chain is expected to change the picture in Fig.3, however, since it bounds the maximum elastic stress that can be exerted by the polymer chain. This is modelled theoretically by the presence of nonlinear terms in the constitutive equation for the polymeric stresses, which limit their growth. Thus while the exponential thinning described in this paper would formally lead to breakup only in infinite time, a real polymer thread does in fact break. Experimental observations of the departure from the exponential law are found for example in Bazilevsky et al. (1997) and Anna & McKinley (2001). The theory in Bazilevsky et al. (1997) differs from the conventional one in that it credits the *degradation* of polymers for the departure from the exponential law.

A number of different nonlinear constitutive equations which bound the maximum polymeric stress have been proposed, and Renardy (Renardy (2001), Renardy (2002)) has considered the asymptotics of a number of different models. A key feature of these analyses is that the thread is predicted to break in finite time when the maximum elastic stress can no longer balance the capillary pressure γ/\bar{h}_{min} . For dilute polymer solutions in particular, the nonlinear form of the force-extension curve close to full extension is well-established both experimentally and theoretically (Li et al. (2000), Shaqfeh et al. (2003)).

Analysis of extensional flow of finitely extensible nonlinear elastic (FENE) dumbbells results in a maximum (dimensionless) polymeric stress of order $\sigma_{zz,max} \approx (2De)Gbv'$ where $b = 3N_K$ is the finite extensibility parameter, which is proportional to the number of Kuhn steps or links (N_K) in the polymer chain. In the elastocapillary necking regime we obtain $(2De)v' = 2/3$ (cf. Figure 9); a naive balance thus suggests that we require $Gb > 2/3$ for elastic effects to be able to grow sufficiently large to balance capillary stresses. A more rigorous balance is substantially more complex and requires a consideration of the initial polymeric stress in the filament and the additional strain accumulated by the fluid in the transient process of the polymeric stress growing to the saturation value $\sigma_{zz,max}$.

Other, more elaborate versions of the FENE model have also been developed (Lhuillier (2001), Ghosh et al. (2002)) which attempt to capture additional features of the internal dynamics of the rapid stretching process for long flexible chains. As the concentration of dissolved polymer chains is increased, entanglement effects also dramatically modify the extensional rheology of the viscoelastic fluid. However, recent experiments have shown that an exponential period of capillary-induced thinning, followed by finite time breakup still occurs (Bhattacharjee et al. (2003)). A significant benefit of the present experimental configuration and accompanying analytical description is precisely that the characteristics of the final breakup process sensitively depend on the nonlinear description of the test fluid that is used. Thus analysis of the capillary-thinning and breakup of polymer solutions provides for a unique testing ground to better understand some of the important nonlinear features of viscoelastic constitutive equations at large strains.

We are grateful to the Deutsche Forschungsgemeinschaft, who funded M. F. and J. L.'s visit to Essen through grant SFB237. G.H.M. and C.C. would like to thank the Dupont-MIT Alliance and the NSF-MRI program for supporting the experimental portion of this work. Daniel Bonn contributed a careful reading of the manuscript and very useful discussions.

Appendix A. Bounds on the velocity

In this appendix we estimate the size of the velocity $v(z_0, t)$ at some reference point z_0 in the crossover region (b) (cf. Figure 10); to this end we integrate (2.1) from the origin of the self-similar region to z_0 :

$$v(z_0, t) = \frac{v(0, t)h^2(0, t) - \int_0^{z_0} (h^2)_t dz}{h^2(z_0, t)} \quad (\text{A } 1)$$

Using the known solution (4.15) one can estimate that the main contribution to the integral

$$I \equiv \int_0^{z_0} (h^2)_t dz$$

comes from the region where $h(z, t)$ is of order $\sqrt{\ell}$, $\ell \equiv \exp[-t/(3De)]$ as usual. We therefore introduce the rescaled profile $\phi(\bar{z})$ by putting

$$h(z, t) = \sqrt{\ell}\phi(\bar{z}), \quad (\text{A } 2)$$

for which (4.15) simplifies to

$$\phi' \approx -\frac{2\phi}{C_1 + 2\phi^2} \quad (\text{A } 3)$$

to leading order in ℓ . Using (A 2) one can compute the time derivative of h to write the integral I as

$$I \approx \frac{\ell^2}{3De} \int_0^{z_0/\ell} (-\phi^2 + \bar{z}(\phi^2)_{\bar{z}}) d\bar{z}.$$

Integration by parts and a change of variables from \bar{z} to ϕ using (A 3) yield

$$\begin{aligned} I &\approx \frac{\ell}{3De} z_0 \phi^2(z_0/\ell) - \frac{2\ell^2}{3De} \int_0^{z_0/\ell} \phi^2 d\bar{z} \\ &\simeq -\frac{2}{3De} z_0^2 + \frac{2\ell^2}{3De} \int_0^{\sqrt{2|z_0|/\ell}} \phi^2 \frac{C_1 + 2\phi^2}{2\phi} d\phi \\ &\simeq -\frac{2}{3De} z_0^2 + \frac{\ell^2}{6De} (C_1 \phi^2 + \phi^4) \Big|_0^{\sqrt{2|z_0|/\ell}} \simeq \frac{C_1 \ell}{3De} |z_0|. \end{aligned}$$

Here we have used that according to (4.18) $\phi(z_0/\ell) \simeq \sqrt{2|z_0|/\ell}$ in the crossover region (b). For simplicity, we also assume that the drop radius $R = 1$.

Having estimated the integral we find from (A 1), using that $h(0, t) \simeq h_0 \ell$ in the neck region,

$$v(z_0, t) \simeq \frac{\frac{L}{3De} h_0^2 \ell^2 - \frac{C_1 \ell}{3De} |z_0|}{2|z_0|} \simeq -\frac{C_1 \ell}{6De} \quad (\text{A 4})$$

as $t \rightarrow \infty$. From this, the derivatives of v are easily estimated as

$$\frac{\partial v}{\partial t}(z_0, t) \simeq \frac{\ell}{18De^2} \quad (\text{A 5})$$

and from (2.1) one finds

$$v_z(z_0, t) = \frac{-v(z_0, t)h_z(z_0, t) - h_t(z_0, t)}{h(z_0, t)} \simeq \frac{\ell}{6De} |z_0| \quad (\text{A 6})$$

Finally, we use (A 4), (A 5), and (A 6) to estimate the different terms of the second equation of (4.7). While for example $\ell^2 \ddot{v} \simeq \ell^3 / De^2$, the curvature term on the right of (4.7) can be estimated as $[\bar{h}^2 K \{\bar{h}\}]' / \bar{h}^2 \simeq \ell^{1/2} / \bar{z}^{3/2}$, which is always much larger in the transition region (b). Therefore the right hand side of (4.7) always dominates the left hand side in the transition region.

REFERENCES

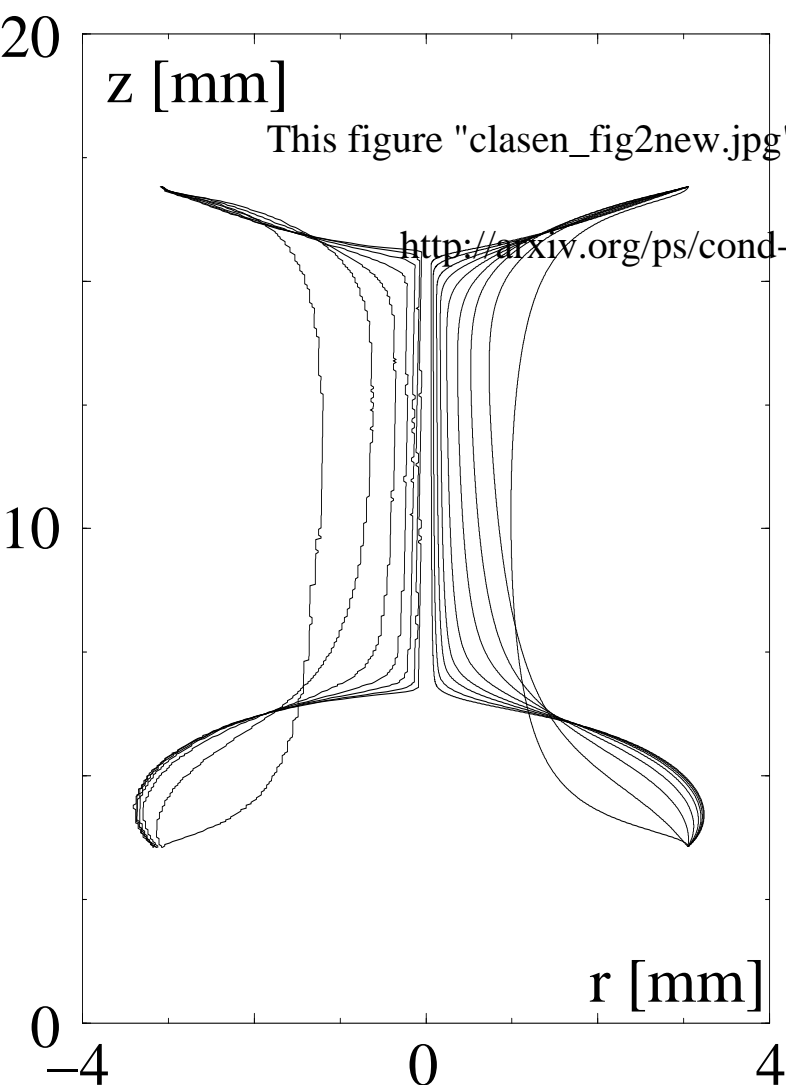
- Amarouchene, Y., Bonn, D., Meunier, J. & Kellay, H. 2001 Inhibition of the finite-time singularity during droplet fission of a polymeric fluid. *Phys. Rev. Lett.* **86**, 3558-3561.
- Anna, S.L. & McKinley, G.H. 2001 Elasto-capillary thinning and breakup of model elastic liquids. *J. Rheol.* **45**, 115-138.
- Bazilevsky, A.V., Entov, V.M., Lerner, M.M. & Rozhkov, A.N. 1997 Failure of polymer solution filaments. *Polym. Sci. Ser. A* **39**, 316-324.
- Bazilevsky, A.V., Entov, V.M., & Rozhkov, A.N. 1990 Liquid Filament Microrheometer and Some of its Applications. Third European Rheology Conference, D. R. Oliver (ed.), Elsevier Applied Science, 41-43.
- Bazilevskii, A.V., Voronkov, S.I., Entov, V.M. & Rozhkov, A.N. 1981 Orientational effects in the decomposition of streams and strands of diluted polymer solutions. *Sov. Phys. Dokl.* **26**, 333-335.
- Bhattacharjee, P.K., Nguyen, D.A., McKinley, G.H. & Sridhar, T. 2003 Extensional Stress Growth and Stress Relaxation in Entangled Polymer Solutions. *J. Rheol.* **47**, 269-290.

- Bird, R.B., Armstrong, R.C. & Hassager O. 1987 *Dynamics of polymeric liquids, Vol. 1: Fluid Mechanics, Vol. 2: Kinetic Theory*. Wiley, New York.
- Bousfield, D.W., Keunings, R., Marrucci, G. & Denn, M.M. 1986 Nonlinear analysis of the surface tension driven breakup of viscoelastic filaments. *J. Non-Newtonian Fluid Mech.* **21**, 79-97.
- Brenner, M.P., Eggers, J., Joseph, K., Nagel, S.D., & Shi, X.D. 1997 Breakdown of scaling in droplet fission at high Reynolds numbers. *Phys. Fluids* **9**, 1573-1590.
- Chang, H.C., Demekhin, E.A. & E. Kalaidin, E. 1999 Iterated stretching of viscoelastic jets. *Phys. Fluids* **11**, 1717-1737.
- Chen, A.U., Notz, P.K., & Basaran, O.A. 2002 Computational and Experimental Analysis of Pinch-Off and Scaling. *Phys. Rev. Lett.* **88**, 174501-4.
- Clasen, C. & McKinley, G.H. 2003, unpublished.
- Christanti, Y.M. & Walker, L. 2001 Surface tension driven jet break up of strain-hardening polymer solutions. *J. Non-Newtonian Fluid Mech.* **100**, 9-26.
- Christanti, Y.M. & Walker, L. 2002 Effect of Fluid Relaxation Time on Jet Breakup due to a Forced Disturbance of Polymer Solutions. *J. Rheol.* **46**, 733-748.
- Cooper-White, J.J., Fagan, J.E., Tirtaatmadja, V., Lester, D.R., & Boger, D.V. 2002 Drop Formation Dynamics of Constant Low Viscosity Elastic Fluids. *J. Non-Newtonian Fluid Mech.* **106**, 29-59.
- Day, R.F., Hinch, E.J., & Lister, J.R. 1998 Self-Similar Capillary Pinchoff of an Inviscid Fluid. *Phys. Rev. Lett.* **80**, 704-712.
- deGennes, P.G. 1979 *Scaling concepts of polymer physics*. Cornell University, Ithaca.
- deGennes, P.G. 1974 Coil-stretch transition of dilute flexible polymers under ultrahigh velocity gradients. *J. Chem. Phys.* **60**, 5030-5042.
- Eggers, J. 1997 Nonlinear dynamics and breakup of free surface flows. *Rev. Mod. Phys.* **69**, 865-929.
- Eggers, J. & Dupont, T.F. 1994 Drop formation in a one-dimensional model of the Navier-Stokes equation. *J. Fluid Mech.* **262**, 205-221.
- Entov, V.M. & Hinch, E.J. 1997 Effect of a spectrum of relaxation times on the capillary thinning of a filament of elastic liquid. *J. Non-Newtonian Fluid Mech.* **72**, 31-53.
- Entov, V.M. & Yarin, A.L. 1984 Influence of Elastic Stresses on the Capillary Breakup of Dilute Polymer Solutions. *Fluid Dyn.* **19**, 21-29, transl. from *Izvestiya Akademii Nauk SSSR, Mekhanika Zhidkosti Gaza* **19**, 27-35.
- Fontelos, M. 2003 Break-up and no break-up in a family of models for the evolution of viscoelastic jets. *ZAMP* **54**, 84-111.
- Fontelos, M. 2002 unpublished.
- Forest, M. G. & Wang, Q. 1990 Change-of-type behavior in viscoelastic slender jet models. *J. Theor. Comp. Fluid Dyn.* **2**, 1-25.
- Funada, T. & Joseph, D.D. 2003 Viscoelastic potential flow analysis of capillary instability. *J. Non-Newtonian Fluid Mech.* **111**, 87-105.
- Goldin, M., Yerushalmi, J., Pfeffer, R. & Shinnar, R. 1969 Breakup of a laminar capillary jet of a viscoelastic fluid. *J. Fluid Mech.* **38**, 689-711.
- Goren, S.L. & Gottlieb, M. 1982 Surface-tension-driven breakup of viscoelastic liquid threads. *J. Fluid Mech.* **120**, 245-266.
- Ghosh, I., Joo, Y.L., McKinley, G.H., Brown, R.A. & Armstrong, R.C. 2002 A New Model for Dilute Polymer Solutions in Flows with Strong Extensional Components. *J. Rheol.* **45**, 1057-1089.
- Kopito, L.E. & Kosasky, H.J. 1979 The Tackiness Rheometer determination of the Viscoelasticity of Cervical Mucus. Human Ovulation, E. S. F. Hafez (ed.), Elsevier/North-Holland, Amsterdam, 351-361.
- Larson, R.G. 1992 Instabilities in viscoelastic flows. *Rheologica Acta* **31**, 213-263.
- Lhuillier, D. 2001 A possible alternative to the FENE dumbbell model of dilute polymer solutions. *J. Non-Newtonian Fluid Mech.* **97**, 87-96.
- Li, J. & Fontelos, M. 2003 Drop dynamics on the beads-on-string structure for viscoelastic jets: A numerical study. *Phys. Fluids* **15**, 922-937.
- Li, L., Larson, R.G. & Sridhar, T. 2000 Brownian Dynamics Simulations of Dilute Polystyrene Solutions. *J. Rheol.* **44**, 291-323.

- Middleman, S. 1965 Stability of a viscoelastic jet. *Chem. Eng. Sc.* **20**, 1037-1040.
- Renardy, M. 1994 Some comments on the surface-tension driven break-up (or the lack of it) of viscoelastic jets. *J. Non-Newtonian Fluid Mech.* **51**, 97-101.
- Renardy, M. 1995 A numerical study of the asymptotic evolution and breakup of Newtonian and viscoelastic jets. *J. Non-Newtonian Fluid Mech.*, **59**, 267-282.
- Renardy, M. 2001 Self-similar breakup of a Giesekus jet. *J. Non-Newtonian Fluid Mech.* **97**, 283-293.
- Renardy, M. 2002 Similarity Solutions For Jet Breakup for Various Models of Viscoelastic Fluids. *J. Non-Newtonian Fluid Mech.* **104**, 65-74.
- Rotherth, A., Richter, R., & Rehberg, I. 2001 Transition from Symmetric to Asymmetric Scaling Function Before Drop Pinch-Off. *Phys. Rev. Lett.* **87**, 4501-4504.
- Shaqfeh, E.S.G., McKinley, G.H., Woo, N., Nguyen, D.A. & Sridhar, T. 2003 On the Polymer Entropic Force Singularity and its Relationship to Extensional Stress Relaxation and Elastic Recoil. *J. Rheol.*, submitted.
- Shipman, R.W.G., Denn, M.M. & Keunings, R. J. 1991 Mechanics of the falling plate extensional rheometer. *J. Non-Newtonian Fluid Mech.*, **40**, 281-288.
- Spiegelberg, S.H., Ables, D.C. & McKinley, G.H. 1996 The role of end-effects on measurements of extensional viscosity in viscoelastic polymer solutions with a filament stretching rheometer. *J. Non-Newtonian Fluid Mech.* **64**, 229-267.
- Stelter, M., Brenn, G., Yarin, A. L., Singh, R. P., & Durst, F. 2000 Validation and Application of a Novel Elongational Device for Polymer Solutions. *J. Rheol.* **44**, 595-616.
- Stokes, Y.M., Tuck, E.O. & Schwartz, L.W. 2000 Extensional fall of a very viscous fluid drop. *Q. J. Mech. Appl. Math.* **53**, 565-582.
- Tripathi, A., Whittingstall, P., & McKinley, G. H. 2000 Using Filament Stretching Rheometry to Predict Strand Formation and "Processability" in Adhesives and Other Non-Newtonian Fluids. *Rheol. Acta* **39**, 321-337.
- von Ohnesorge, W. 1936 Die Bildung von Tropfen an Düsen und die Auflösung flüssiger Strahlen. *ZAMM* **16**, 355-358.
- Yarin, A.L. 1993 *Free liquid jets and films: Hydrodynamics and rheology*. Wiley, New York.

This figure "Fig1_small.JPG" is available in "JPG" format from:

<http://arxiv.org/ps/cond-mat/0307611v1>



This figure "clasen_fig2new.jpg" is available in "jpg" format from:

<http://arxiv.org/ps/cond-mat/0307611v1>

